Meteoritics & Planetary Science 32, 825–840 (1997)

Vesta as the howardite, eucrite and diogenite parent body: Implications for the size of a core and for large-scale differentiation

ALEX RUZICKA*, GREGORY A. SNYDER AND LAWRENCE A. TAYLOR

Planetary Geosciences Institute, Department of Geological Sciences, University of Tennessee, Knoxville, Tennessee 37996-1410
Correspondence author's e-mail address: aruzicka@utk.edu

(Received 1996 December 10; accepted in revised form 1997 May 29)
(Presented at the Workshop on Vesta and the HED Meteorites, Houston, Texas, USA, 1996 October 16–18)
(Dedicated to the memory of Paul Pellas)

Abstract–If Vesta is the parent body of the howardite, eucrite, and diogenite (HED) meteorites, then geochemical and petrologic constraints for the meteorites may be used in conjunction with astronomical constraints for the size and mass of Vesta to (1) determine the size of a possible metal core in Vesta and (2) model the igneous differentiation and internal structure of Vesta.

The density of Vesta and petrologic models for HED meteorites together suggest that the amount of metal in the parent body is <25 mass%, with a best estimate of ~5%, assuming no porosity. For a porosity of up to 5% in the silicate fraction of the asteroid, the permissible metal content is <30%. These results suggest that any metal core in the HED parent body and Vesta is not unusually large.

A variety of geochemical and other data for HED meteorites are consistent with the idea that they originated in a magma ocean. It appears that diogenites formed by crystal accumulation in a magma ocean cumulate pile and that most noncumulate eucrites (excepting such eucrites as Bouvante and Stannern) formed by subsequent crystallization of the residual melts. Modelling results suggest that the HED parent body is enriched in rare earth elements by a factor of ~2.5–3.5 relative to CI-chondrites and that it has approximately chondritic Mg/Si and Al/Sc ratios. Stokes settling calculations for a Vesta-wide, nonturbulent magma ocean suggest that early-crystallizing magnesian olivine, orthopyroxene, and pigeonite would have settled relatively quickly, permitting fractional crystallization to occur, but that later-crystallizing phases would have settled (or floated) an order of magnitude more slowly, allowing, instead, a closer approach to equilibrium crystallization for the more evolved (eucritic) melts. This would have inhibited the formation of a plagioclase-flotation crust on Vesta.

Plausible models for the interior of Vesta, which are consistent with the data for HED meteorites and Vesta, include a metal core (<130 km radius), an olivine-rich mantle (~65–220 km thick), a lower crustal unit (~12–43 km thick) composed of pyroxenite, from which diogenites were derived, and an upper crustal unit (~23–42 km thick), from which eucrites originated. The present shape of Vesta (with ~60 km difference in the maximum and minimum radius) suggests that all of the crustal materials, and possibly some of the underlying olivine from the mantle, could have been locally excavated or exposed by impact cratering.

INTRODUCTION

Meteorites belonging to the howardite, eucrite, and diogenite (HED) clan are believed to have originated on the same parent body, based on common O isotopic compositions (Clayton and Mayeda, 1996), the coexistence of eucrite- and diogenite-like lithologies in polymict breccias (*e.g.*, Duke and Silver, 1967; Bunch, 1975; Mason *et al.*, 1979), and an apparent continuum in mineral assemblages and compositions between diogenitic material (orthopyroxenites) to eucritic material (gabbro and basalt) (*e.g.*, Duke and Silver, 1967). There are good reasons to believe that the HED parent body is asteroid 4 Vesta. This includes remote spectroscopic evidence that suggests that Vesta alone among all large main-belt asteroids resembles HED meteorites (*e.g.*, Consolmagno and Drake, 1977; Gaffey *et al.*, 1989). In addition, there is the recent discovery of 26 small (4–10 km in diameter) asteroids ("Vestoids") with Vesta-like reflectance spectra in a variety of orbits between Vesta and dynamical resonances in the asteroid belt (Binzel and Xu, 1993). The existence of these Vestoids imply that material is being removed from Vesta and transported to dynamical resonance locations, from where it can be perturbed into Earth-crossing orbits (Binzel and Xu, 1993; Binzel, 1996).

Based on this evidence, it appears that the HED meteorites belong to a relatively exclusive group of meteorites for which the identity of the parent body is believed to be known. Moreover, the variety and large number of HED meteorites in our collections suggest that the igneous lithologies in the parent body were unusually well sampled. Only olivine and possibly metal from the parent body may be largely missing in the sample collections. These considerations suggest that combined studies of Vesta and HED meteorites might prove to be especially insightful for understanding the origin of Vesta.

Howardites are polymict breccias composed of clasts of diogenite- and eucrite-like material and appear to have formed largely as mixtures of diogenites and eucrites in the regolith of the HED parent body (*e.g.*, Duke and Silver, 1967; Chou *et al.*, 1976; Dreibus *et al.*, 1977). Diogenites are unbrecciated, monomict, or polymict orthopyroxenites that originally formed as cumulates in one or more magmas undergoing fractional crystallization (*e.g.*, Fukuoka *et al.*, 1977; Mittlefehldt, 1994; Fowler *et al.*, 1994, 1995). Eucrites are unbrecciated, monomict, or polymict breccias that can be subdivided into "cumulate eucrites," including cumulate-feldspar eucrites and cumulate-pigeonite (Binda-type) eucrites, and into "noncumulate eucrites." As the name implies, the cumulate eucrites are believed to have formed as cumulates during fractional crystallization (*e.g.*, Stolper, 1977; Consolmagno and Drake, 1977; Hamet *et al.*, 1978). The origin of noncumulate eucrites is more obscure. They may have originally formed in one of two ways, either as (1) partial (primary) melts of the HED parent body that experienced comparatively little modification by fractional crystallization processes (Stolper, 1977;

Consolmagno and Drake, 1977; Jones, 1984, Jurewicz *et al.*, 1993), or (2) melts produced from the same or similar magmas that had earlier crystallized diogenites (Mason, 1967; Warren, 1985; Ikeda and Takeda, 1985; Warren and Jerde, 1987; Hewins and Newsom, 1988; Grove and Bartels, 1992). The large and apparently continuous variations in mineral compositions and mineral assemblages in howardites and polymict eucrites (*e.g.*, Duke and Silver, 1967; Delaney *et al.*, 1984; Takeda and Mori, 1985; Ikeda and Takeda, 1985) provide compelling evidence for the importance of fractionating magmas in the HED parent body. However, the role that fractional crystallization may have played in the origin of noncumulate eucrites is still being debated.

Most studies of eucrites have concluded that the HED parent body is poor in volatile elements but otherwise is generally chondritic in composition (*e.g.*, Dreibus *et al.*, 1977; Morgan *et al.*, 1978). It is generally believed that metal segregation occurred in the parent body to form a core (Hewins and Newsom, 1988). Siderophile element depletions in eucrites have been modelled to infer the amount of metal that segregated into a core and the degree of partial melting during metal segregation. Estimates of the amount of metal in the HED parent body, based on the siderophile element depletions in eucrites, vary widely: 13% (Morgan *et al.*, 1978), 32–42% (Palme and Rammensee, 1981), 2–10% (Newsom and Drake, 1982), 7–35% (Newsom and Drake, 1983), 30–50% (Newsom, 1985), 15–45% (Jones *et al.*, 1988), 20–40% (Hewins and Newsom, 1988), and 6–22% (Righter and Drake, 1997a). Metal contents in chondrites rarely exceed ~20 wt% (*e.g.*, Jarosewich, 1990), and some of the estimates for the metal content in the HED parent body imply superchondritic metal contents.

In this paper, we assume that Vesta is the HED parent body. We then use astronomical constraints for the size and mass of Vesta, in conjunction with geochemical and petrologic data for HED meteorites, to model the interior structure and igneous evolution of the asteroid. We estimate the amount of metal in the asteroid, using an approach independent of that based on models of siderophile element depletions in eucrites. Our results suggest that (1) an unusually large amount of metal is not present in Vesta, (2) the HED suite originated in a magma ocean (Ikeda and Takeda, 1985), and (3) Vesta fully differentiated to produce a layered core-mantle-crust structure.

SIZE OF METAL CORE IN VESTA

Siderophile-element depletions in HED meteorites imply that the HED parent body experienced metal segregation, which suggests the formation of a metallic core. If Vesta is the HED parent body, astronomical constraints for the overall density of Vesta can be combined with estimates of the density of the silicate fraction of Vesta to determine the size of a metal core by mass balance.

Bulk Density of Vesta

The density of Vesta can be inferred from astronomical constraints for the mass and radius of the asteroid (Table 1). Independent values for the mass of Vesta have been determined by Schubart and Matson (1979) and Standish and Hellings (1989), based on analyzing the perturbations by Vesta on two different objects: asteroid Arrete and the planet Mars. Although the masses for Vesta determined by these workers ($2.75 \pm 0.24 \times 10^{23}$ g and $3.0 \pm 0.6 \times 10^{23}$ g, respectively) overlap, the former value is used here, as it is more precise. Undoubtedly, the best estimates for the radius of Vesta are based on recent Hubble Space Telescope (HST) data (Thomas *et al.*, 1996; Thomas, pers. comm., 1996). Thomas *et al.* (1996) reported

TABLE 1. Physical parameters for Vesta.

mass*	$2.75 \pm 0.24 \times 10^{23}$ g
radius†	$289 \times 280 \times 229 \pm 7$ km
density	3.54 ± 0.42 g/cm^3
surface gravity	~0.26 m/s^2
pressure at center	~1.2 kb

*Schubart and Matson (1979).
†Thomas, pers. comm. (1996).

that the shape of Vesta is approximately that of an ellipsoid with radii of 280 × 272 × 227 km and an estimated error of ±12 km for the radius in each dimension. These radii values were subsequently revised to 289 × 280 × 229 ± 7 km (Thomas, pers. comm., 1996). Based on the latest HST data, the mean radius of Vesta is ~266 km, and the radius of a sphere with equivalent volume to that of Vesta is ~265 km. These data agree with previous estimates for the average radius of Vesta (269 ± 14 km, Morrison, 1977; 272 ± 40 km, Schubart and Matson, 1979). Thus, it appears that both the mass and radius of Vesta are reliably determined. Using the mass of Schubart and Matson (1979) and the revised radii of Thomas (pers. comm., 1996), the density of Vesta is 3.54 ± 0.42 g/cm^3 (Table 1).

It should be noted that the quoted error on the density is a "$\pm 1\sigma$ error," which is obtained by propagating an assumed error of ±7 km radius in each of three orthogonal directions to an error in the calculated volume and propagating this error in volume with the quoted error in the mass. Unless the average small-scale relief on Vesta is >14 km, the assumed error in the volume will be larger than any volume uncertainty introduced by the local topography.

Mass Balance and Porosity Considerations

For a two-component mixture of metal and silicate in Vesta, mass balance implies

$$\chi_{metal} = \frac{\rho_{Vesta} - \rho_{silicate}}{\rho_{metal} - \rho_{silicate}} \quad \text{Eq. (1)}$$

and

$$X_{metal} = \frac{\rho_{metal}}{\rho_{Vesta}} \left[\frac{\rho_{Vesta} - \rho_{silicate}}{\rho_{metal} - \rho_{silicate}} \right] \quad \text{Eq. (2)}$$

where χ_{metal} = volume fraction metal in Vesta, X_{metal} = mass fraction of metal in Vesta, ρ_{Vesta} = density of Vesta, ρ_{metal} = density of the metal component, and $\rho_{silicate}$ = density of the silicate component.

The bulk densities of the metal and silicate components will be decreased by the presence of porosity. Porosity may be important in small asteroids (Britt and Consolmagno, 1997), but whether a large asteroid such as Vesta can have significant overall porosity is debatable. Self-compression in a large asteroid such as Vesta will tend to minimize porosity.

Vesta has a central pressure of ~1 kb (Table 1), and porosity will be minimized near the center of the asteroid where self-compression is highest. Thus, we assume negligible porosity associated with a metal core in Vesta and take $\rho_{metal} = 7.87$ g/cm^3, which is appropriate for kamacite (BVSP, 1981). Although S and Ni are likely to be present in any metal core in addition to Fe, we have not attempted to model the addition of these elements, largely because their concentrations in a core are poorly known. However, the simultaneous addition of both components to a core will tend to leave the value of ρ_{metal} relatively unchanged, as S will lower while Ni will raise the density of the core.

The bulk density of the silicate fraction can be expressed as

$$\rho_{silicate} = (1 - \phi)\rho_{mineral} \quad \text{Eq. (3)}$$

where ϕ is the volume fraction of pores (0–1) in the silicate fraction and $\rho_{mineral}$ is the density of the mineral assemblage. The mineral assemblage can be inferred from petrological and geochemical models of HED meteorites. Consequently, $\rho_{mineral}$ can, in principle, be determined. In calculating $\rho_{mineral}$, the following mineral densities (in grams per cubic centimeter, from Deer *et al.*, 1966) were assumed: pigeonite 3.30–3.46, orthopyroxene 3.21–3.96, augite 2.96–3.52, olivine 3.22–4.39, plagioclase 2.63–2.76, tridymite 2.26, chromite 5.09, and ilmenite 4.74. Interpolation was used to determine the density of minerals in solid-solution series.

A plausible value for ϕ in Eq. (3) can be inferred based on porosity measurements of various meteorites (Britt and Consolmagno, 1997), although such data must be used with discretion, as the porosities of meteorites are likely to have been strongly influenced both by impact shock and terrestrial weathering processes. Juvinas, the one HED sample measured by Britt and Consolmagno (1997), has a porosity of ~10% (ϕ = 0.10). Sixteen ordinary chondrites, which arguably have a mineralogy (although probably not a texture) similar to that of Vesta, range in porosity from 0.3 to 17%, with the higher porosities corresponding to weathered specimens (Britt and Consolmagno, 1997). From this data set, we consider values of $\phi \leq 0.05$ to be plausible for the silicate fraction of Vesta, although we suspect that the actual value of ϕ for Vesta is in the range of 0–0.02.

Using Eq. (2), Fig. 1 shows the inferred metal mass fraction in Vesta for a given value of $\rho_{silicate}$ and for three different values of ρ_{Vesta} corresponding to the lower-limit, the best-estimate, and the upper-limit of the latter parameter. From Eq. (3), $\rho_{mineral} = \rho_{silicate}$ when ϕ = 0, and $\rho_{silicate} = 0.95 \times \rho_{mineral}$ when ϕ = 0.05. Once $\rho_{mineral}$ and ϕ are specified, $\rho_{silicate}$ can be calculated, and Fig. 1 can be used to determine the metal content of Vesta.

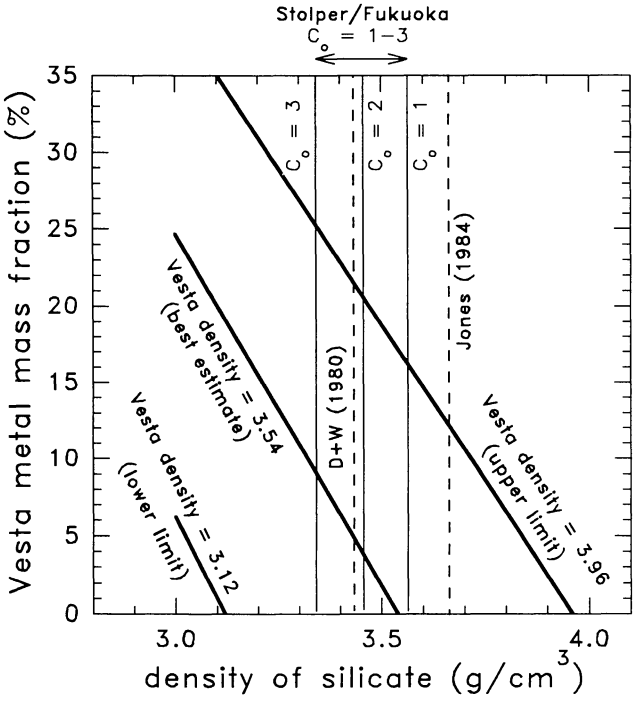

FIG. 1. Metal mass fraction in Vesta as a function of the density of the silicate portion ($\rho_{silicate}$) for three values of the bulk density of Vesta (ρ_{Vesta} = 3.12 g/cm^3, 3.54 g/cm^3, and 3.96 g/cm^3, corresponding to the lower-limit, the best-estimate, and the upper-limit, respectively.) Vertical lines show the value of $\rho_{silicate}$ for various parent body composition models (Jones, 1984; Dreibus and Wänke, 1980; and Stolper/Fukuoka) assuming negligible porosity in Vesta. For the Stolper/Fukuoka models, three values of the parameter C_o (= CI-normalized abundance of refractory lithophile elements) are shown; a value of $C_o \sim 2$ is probably most appropriate for these models. For a density of 3.54 g/cm^3 and a value for $\rho_{silicate}$ of ~3.45 g/cm^3, the metal mass fraction in Vesta would be ~5%.

Density of the Silicate Fraction in Vesta—Model 1

Model 1 assumes that the source region of the eucrites is identical to the silicate fraction of Vesta. Implicit in this model is the notion that at least some eucrites originated as relatively simple products of partial melting within the HED parent body.

Utilizing mineral-melt partition coefficients for Sc, Mg, and Si, Jones (1984) modelled the composition of the eucrite parent body as consisting of 75% olivine and 25% Main Group eucrite, with eucrites formed by roughly 25% partial melting. The CIPW norm of the eucrite parent body composition of Jones (1984) is as follows: 74.6 wt% olivine (Fo_{57}), 11.9% orthopyroxene (En_{59}), 9.2% plagioclase ($An_{89}Or_1$), 3.7% clinopyroxene ($Wo_{50}En_{29}$), 0.3% ilmenite, and 0.3% chromite. Assuming that this norm approximates the actual mineralogy of the source, an overall value for $\rho_{mineral}$ = 3.63 g/cm^3 is implied. Assuming ϕ = 0 and the upper-limit density of Vesta, this corresponds to a metal mass fraction in Vesta of <15% (Fig. 1). For ϕ = 0.05, the metal mass fraction is <23%.

Melting experiments by Stolper (1977) suggested that eucrites formed by partial melting of a source region consisting mainly of olivine (Fo_{65}), low-Ca pyroxene (Wo_5En_{65}), and plagioclase (An_{94}), and Fukuoka *et al.* (1977) modelled trace-element (La, Sm, Yb, Sc, Sr, and Ba) abundances of the Sioux County and Stannern eucrites with a partial-melting model. The latter authors found that different proportions of olivine, low-Ca pyroxene, and plagioclase in the source region could be accommodated depending on the value of a parameter, C_o, which is equal to the CI-chondrite normalized concentration of trace refractory lithophile elements in the source region. The larger the value of C_o, the less olivine in the source. The depletion of volatile lithophile elements in HED meteorites compared to chondrites (Dreibus *et al.*, 1977; Morgan *et al.*, 1978) implies that refractory lithophile elements are enriched in the parent body (*i.e.*, $C_o > 1$). On the other hand, a value of C_o much greater than 3 for Model 1 would imply no olivine in the eucrite source region, which is inconsistent with the models of Stolper (1977) and Fukuoka *et al.* (1977). Thus, values of C_o ranging from ~1–3 are permissible for the Stolper/Fukuoka models.

As C_o increases from 1 to 3, the proportion of olivine in the source region decreases from ~85 to ~8%, the proportion of low-Ca pyroxene increases from ~11 to ~80%, and the proportion of plagioclase increases from ~4 to ~12%, with a net decrease in $\rho_{mineral}$ from ~3.58 to ~3.32 g/cm^3. Assuming ϕ = 0, a metal mass fraction of 0–27% in Vesta is inferred based on the Stolper/Fukuoka models (Fig. 1). The higher metal contents for the latter require simultane-ously extreme assumptions about the density of Vesta (ρ_{Vesta} = 3.96 g/cm^3, the upper limit) and the composition of the eucrite source region (C_o = 3, the upper limit). Jones *et al.* (1990) suggested that the most appropriate source composition for a eucrite partial melting model has $C_o \sim 2$. In this case, $\rho_{mineral}$ is ~3.46 g/cm^3 based on the Stolper/Fukuoka models. For C_o = 2 and ϕ = 0, the metal mass fraction in Vesta is ~4%, with an upper limit of ~23% (Fig. 1). For ϕ = 0.05, this becomes ~12% with an upper limit of ~29%.

Density of the Silicate Fraction in Vesta—Model 2

In Model 2, the silicate portion of Vesta is composed of a mixture of HED materials and olivine, as proposed by Dreibus *et al.* (1977) and Dreibus and Wänke (1980). These authors varied the proportion of eucrite and diogenite in the parent body until a chon-

dritic Al/Sc ratio was obtained and then added olivine (assumed by Dreibus and Wänke (1980) to be equivalent to olivine in a pallasite meteorite) to the mixture, so as to obtain a chondritic Mg/Si ratio. Chondritic ratios of Al/Sc and Mg/Si for the HED parent asteroid are reasonable, as ratios of nonvolatile lithophile elements in the HED parent body appear to be roughly chondritic (Dreibus *et al.*, 1977; Morgan *et al.*, 1978; Wänke, 1981; Warren, 1983). Model 2 is not tied to any specific petrogenetic model, but it implicitly assumes that the parent body was differentiated into an unsampled (and presumably deep) olivine-rich portion and a well-sampled (and presumably near-surface) portion containing eucritic, howarditic, and diogenitic material.

The CIPW norm of the Dreibus and Wänke (1980) parent body composition has 48.5 wt% olivine (Fo_{72}), 38.2% orthopyroxene (En_{79}), 9.5% plagioclase ($An_{94}Or_{0.3}$), 3.5% clinopyroxene (Wo_{50} En_{39}), and 0.3% ilmenite. Assuming that this norm is representative of the mineralogy, $\rho_{mineral}$ is 3.42 g/cm^3. For $\phi = 0$, this corresponds to a metal mass fraction of ~6%, with an upper limit of ~24% (Fig. 1). For $\phi = 0.05$, the inferred metal mass fraction is increased to ~14%, with an upper limit of ~30%.

Size of Metal Core in Vesta

Models 1 and 2 give consistent results for the density of the silicate fraction in the HED parent body ($\rho_{mineral}$ ~ 3.32–3.63 g/cm^3), and this leads to consistent estimates for the size of a metal core in Vesta. For negligible values of porosity, the metal content is inferred to be in the range of ~0–10 mass% (~0–4 vol%) for reasonable values of parent body composition and likely values for the bulk density of Vesta, although metal contents as high as 25 mass% cannot be excluded. If up to 5% porosity in the silicate fraction of the asteroid is allowed and the actual bulk density of Vesta is close to the inferred upper limit, metal contents as high as ~30 mass% are possible. These metal contents are within the range observed for chondrites.

Estimates of the amount of metal in Vesta and the HED parent body based on this work are summarized in Fig. 2 where they are compared to literature estimates for the amount of metal in the eucrite parent body based on modelling siderophile-element depletions in eucrites. In Fig. 2, the best estimates shown for Models 1 and 2 (~4% and ~6% metal, respectively) assume the best-estimate value for the density of Vesta, negligible porosity, and (for Model 1) reasonable estimates of parent body composition, while the ranges show the effect of more extreme assumptions regarding these parameters. Even with the fairly large uncertainties inherent in the approach used here, it is clear that the data are inconsistent with many of the literature estimates, which call for metal contents as high as 50 mass% (Fig. 2). On the other hand, some literature estimates for the size of a metal core in the eucrite parent body, in particular those by Morgan *et al.* (1978), Newsom and Drake (1982), and Righter and Drake (1997a), are consistent with the estimates of the metal content in Vesta deduced here (Fig. 2). Based on our results, a superchondritic metal content in Vesta seems unlikely.

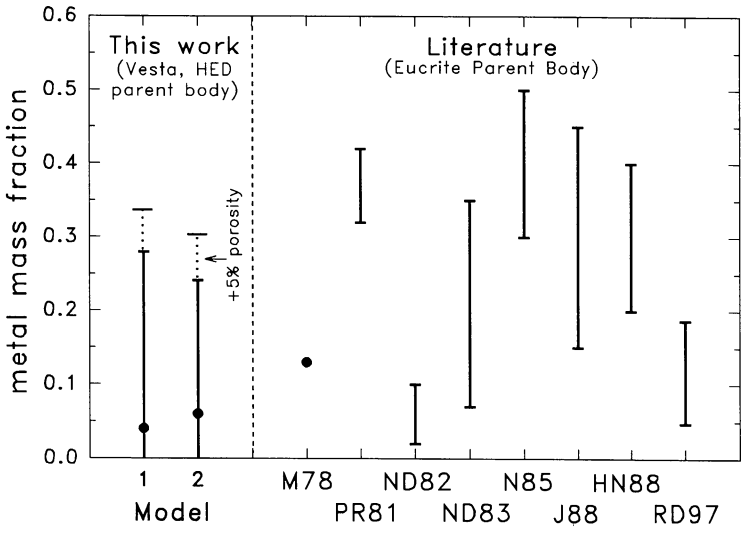

FIG. 2. Metal mass fraction in Vesta and the HED parent body (this work) compared to estimates in the literature for the eucrite parent body based on modelling siderophile element depletions. M78 = Morgan *et al.* (1978); PR81 = Palme and Rammensee (1981); ND82 = Newsom and Drake, 1982; ND83 = Newsom and Drake (1983); N85 = Newsom (1985); J88 = Jones *et al.* (1988); HN88 = Hewins and Newsom (1988); RD97 = Righter and Drake (1997a). The RD97 range corresponds to the metal present in a core that also contains sulfide (Righter and Drake, 1997a).

DIFFERENTIATION AND INTERNAL STRUCTURE OF VESTA

In this section, we model the differentiation and interior of Vesta assuming that it is the HED parent body. Our modelling results support the hypothesis that the HED meteorites originated in a magma ocean (Ikeda and Takeda, 1985) and that the parent body differentiated extensively (Takeda, 1996). Takeda and coworkers have long suggested that the HED suite could have been derived from a layered crust formed by fractional crystallization, with noncumulate eucrites respectively overlying cumulate eucrites and diogenites (Takeda *et al.*, 1976, 1979; Miyamoto and Takeda, 1977, 1994). Similarly, Delaney (1995) discussed the possibility that HED meteorites could have crystallized in a Vestan "magma spheroid" created by a "small giant impact" between colliding objects. More recently, Ruzicka *et al.* (1997a,b) and Righter and Drake (1997b) argued that a magma ocean could explain many of the geochemical characteristics of HED-suite meteorites, and Lugmair and Shukolyukov (1997) suggested that an early, global differentiation episode on the HED parent body was consistent with Mn-Cr isotopic data for eucrites and diogenites.

Melt Compositions

In the magma ocean models discussed below, it is necessary to assume an initial composition for the melt. The approach of Dreibus and Wänke (1980) was used, as it depends on relatively few assumptions, and as the assumptions that are made are reasonable. The key assumptions are that (1) the Al/Sc and Mg/Si ratios of the parent body are the same as those in chondrites and that (2) the silicate portion of the parent body is composed of a mixture of eucrites, diogenites, and olivine. Implicit in the second assumption is that, except for olivine, the silicate portion of the parent body was well sampled by HED-suite meteorites. The first assumption is reasonable if the parent body formed largely out of chondritic materials. The second assumption is also reasonable, as the HED suite consists of many breccias but only two principal lithologies (eucrites and diogenites).

Once the compositions for the eucrite, diogenite, and olivine endmembers are specified, the three components can be mixed so as to obtain Al/Sc and Mg/Si ratios of any particular chondrite type. This mixture then represents the assumed composition of the parent body and the initial melt. Our approach differs slightly from Dreibus and Wänke

(1980) in that the Sc content of the assumed olivine component is included in the mixing computation, whereas it was neglected by the former authors. However, our mixing calculations utilize the same olivine component and similar eucrite and diogenite components as Dreibus and Wänke (1980).

In Table 2, we show hypothetical HED parent compositions assuming Al/Sc and Mg/Si ratios identical to carbonaceous, ordinary, and enstatite chondrites. Chondrites have relatively uniform Al/Sc ratios but vary in Mg/Si ratios, with the latter being highest in carbonaceous chondrites and lowest in enstatite chondrites. This difference in Mg/Si ratios manifests itself as various amounts of olivine in the parent body compositions shown in Table 2. Thus, a carbonaceous chondrite protolith results in a relatively olivine-rich parent body, whereas an enstatite chondrite protolith results in an olivine-poor parent body (Table 2).

Mineralogy and Pyroxene Compositions

We used the MAGFOX program, written by J. Longhi, to model fractional crystallization in an HED magma ocean. The program determines the mineralogy and mineral compositions of cumulates, and the corresponding major-element compositions of melts, produced by fractional crystallization. In our models, the initial compositions given in Table 2 were used as inputs to MAGFOX.

Table 3 shows the mineral assemblages that are produced by successive crystallization at 1 bar of the HED-CI model magma, although similar results are obtained for all of the compositions given in Table 2. The amount of olivine that crystallizes will be greatest for a carbonaceous-chondrite-like protolith and smallest for an enstatite-chondrite-like protolith, but otherwise, identical assemblages and virtually identical mineral compositions are obtained for the different precursors. Different stages are identified in Table 3 that correspond to changes in mineral assemblages. To facilitate discussion, reference will be made to these stages throughout the remainder of this paper.

Fractional crystallization of an HED magma ocean is expected to result first in olivine alone (initial-stage 1), followed by orthopyroxene ± chromite (stage 1–3), and then by pigeonite alone (stage 3–4) (Table 3). Although chromite is predicted to cocrystallize with orthopyroxene, the phase equilibria involving chromite are inadequately handled by the program (J. Longhi, pers. comm.). Thus, the model results for chromite should be considered highly tentative. Plagioclase begins to crystallize at stage 4. Continued fractional crystallization will produce plagioclase, pigeonite, silica polymorph, ferrous olivine, and augite (Table 3). Ilmenite joins the crystallization sequence after solidification is essentially (~99%) complete (stage 7).

One of the characteristics of fractional crystallization is the formation of cumulates that have widely varying mineral compositions. Figure 3 shows that the composition of the model pyroxene in the cumulates becomes increasingly ferrous and calcic as crystallization progresses. The composition ranges from magnesian orthopyroxene ($En_{83-76}Wo_{1-2}$) between stages 1–3, to pigeonite (En_{75-39}, Wo_{2-8}) between stages 3–6, and finally to augite ($En_{29-0}Wo_{33-36}$) between stages 6–7.

The pyroxene cumulates that form between stages 1 and 3 resemble diogenites in mineralogy. Diogenites consist primarily of orthopyroxene (En_{79-66}, mainly En_{74}; Mittlefehldt, 1994; Fowler *et al.*, 1994) and have an average mode of ~92% orthopyroxene, ~4% olivine, ~1% clinopyroxene, ~0.9% chromite, and ~2% other (Bowman *et al.*, 1996). The mineralogy of stage 1–3 orthopyroxene cumulates resembles diogenites, with the notable exception that olivine abundances are higher in diogenites. The excess olivine can be explained by incomplete settling of earlier-crystallized olivine. Chromite abundances in diogenites are lower on average than what

TABLE 2. Model compositions of the HED parent body, derived using the procedure of Dreibus and Wänke (1980) but for various chondrite-like protoliths.

	DW80 (1)	HED-CI (2)	HED-CM (3)	HED-L (3)	HED-EH (3)
protolith	CI	CI	CM	L	EH
wt%					
SiO_2	46.23	45.34	45.74	46.96	49.06
TiO_2	0.16	0.18	0.18	0.21	0.26
Al_2O_3	3.27	3.29	3.25	3.71	4.63
Cr_2O_3	0.91	0.85	0.88	0.92	0.98
FeO	14.79	14.34	14.48	15.11	16.25
MnO	0.42	0.40	0.41	0.44	0.49
MgO	31.53	32.67	32.16	29.30	24.15
CaO	2.57	2.78	2.76	3.17	3.97
Na_2O	0.11	0.12	0.12	0.14	0.17
K_2O	0.01	0.01	0.01	0.01	0.01
P_2O_5	–	0.02	0.02	0.03	0.04
at%					
Mg/(Mg + Fe)	79	80	80	78	73
wt/wt					
MgO/SiO_2	0.68	0.72	0.70	0.62	0.49
CaO/Al_2O_3	0.79	0.84	0.85	0.85	0.86
FeO/MnO	35	36	35	34	33
mass%					
eucrite	–	24.3	23.7	26.8	33.1
diogenite	–	24.3	27.8	35.3	47.2
olivine	43	51.4	48.5	37.9	19.7

References: (1) Dreibus and Wänke (1980); (2) bulk Al/Sc and Mg/Si as in CI chondrites (Anders and Grevesse, 1989); olivine composition as in Dreibus and Wänke (1980); (3) bulk Al/Sc and Mg/Si as in CM, L and EH chondrites (Wasson and Kallemeyn, 1988); olivine composition as in Dreibus and Wänke (1980).

TABLE 3. Low-pressure (1 bar) fractional crystallization sequence of a Vesta-wide magma ocean, based on the MAGFOX program developed by J. Longhi, assuming a parent body composed of eucrite + diogenite + olivine with CI-like Al/Sc and Mg/Si ratios (HED-CI model).

Stage	Vol% crystallized	Assemblage*
1	0–61	ol (Fo_{93-80})
2	61–64	opx ($En_{83-80}Wo_{1.1-1.3}$)
3	64–69	90% opx ($En_{80-76}Wo_{1.3-2.1}$) +10% chr†
4	69–77	pig ($En_{75-59}Wo_{2-5}$)
5	77–87	62% plag (An_{93-91}) +38% pig ($En_{59-41}Wo_{5-7}$)
6	87–90	56% plag (An_{91-90}) +10% pig ($En_{41-39}Wo_{7-8}$) + 27% ol (Fo_{37-33}) + 7% silica
7	90–99	48% plag (An_{90-71}) + 27% aug ($En_{28-0}Wo_{33-36}$) + 20% ol (Fo_{33-0}) + 5% silica
	99	

*Modes in vol%. ol = olivine; opx = orthopyroxene; chr = chromite; pig = pigeonite; plag = plagioclase; aug = augite; silica = silica polymorph.
†Probable overestimate (see text).

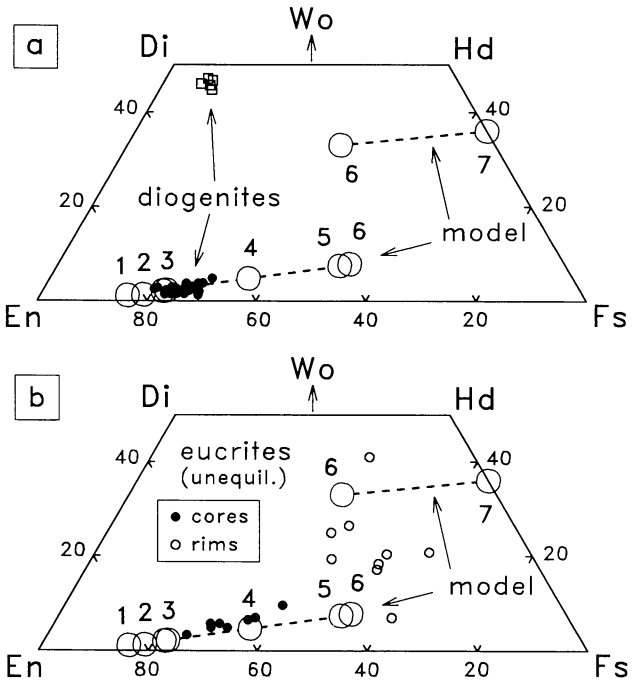

FIG. 3. Pyroxene quadrilateral diagrams showing the average compositions of pyroxenes found in diogenites (Mittlefehldt, 1994; Fowler *et al.*, 1994) and in unequilibrated eucrites (Miyamoto *et al.*, 1985; Pun and Papike, 1996) compared to model predictions for fractional crystallization in an HED magma ocean. The numbers associated with the model track correspond to the stages shown in Table 3, with 1 being the first pyroxene to crystallize and 7 being the last. "Core" and "rim" compositions for eucrites refer to grain cores and rims, respectively.

would be predicted by the model, and this probably reflects a tendency for MAGFOX to overestimate the amount of chromite that will crystallize early with orthopyroxene.

Pyroxene compositions in diogenites follow the compositional track predicted by the model, passing through stage 3 between stages 2 and 4 (Fig. 3). The pyroxene in diogenites is largely orthopyroxene (Mittlefehldt, 1994; Fowler *et al.*, 1994, 1995), and in the model, orthopyroxene ceases to crystallize at stage 3, and pigeonite begins to crystallize at stage 3. Yet the composition of diogenitic pyroxene does not merely extend *to* stage 3 but rather extends *beyond* it (Fig. 3). This indicates an apparent discrepancy between the model and the observations. The discrepancy could indicate either that (1) some of the pyroxene in diogenites actually crystallized as pigeonite initially and subsequently inverted to a mixture of orthopyroxene and augite, or that (2) the composition of the diogenite orthopyroxene was affected by a reequilibration process that increased the Fe and Ca content of the pyroxene. There is support for each of these alternatives. Some augite occurs in diogenites (Fig. 3; Mittlefehldt, 1994), and such augite could conceivably have inverted from an early formed pigeonite. Similarly, a reequilibration process has been inferred for diogenites from the tendency for the abundances of Mg and Fe in orthopyroxene to be more uniform than for presumably less mobile elements, such as Al, Ti, and the rare earth elements (Mittlefehldt, 1994; Fowler *et al.*, 1994, 1995). The tendency for diogenite pyroxene compositions to lie at a more evolved point on the crystallization trend than might otherwise be expected (Fig. 3) is consistent with a reequilibration hypothesis, in which earlier-formed pyroxene exchanged components with a surrounding melt that continued to evolve.

Taken as a whole, the data suggest that diogenites could correspond to stage 1–3 cumulates that have an admixture of olivine and that experienced limited reequilibration with a more evolved melt.

Following orthopyroxene crystallization, pigeonite alone crystallizes between stages 3 and 4. The composition of this pigeonite is similar to the compositions of pigeonite grain cores in unequilibrated (weakly metamorphosed) eucrites (Fig. 3). This suggests that the cores of pyroxene grains in unequilibrated eucrites could have been in equilibrium with melts that formed soon after diogenites were produced. The rims of pyroxene grains in unequilibrated eucrites have compositions that resemble a mixture of the pigeonite and augite that is expected to crystallize around stage 6 (Fig. 3), which implies that these rims could have equilibrated with melts that evolved to stage 6. There is a tendency for the grain cores in unequilibrated eucrites to have compositions that are slightly more calcic than predicted (Fig. 3), and this could indicate that these cores experienced limited equilibration with more evolved, calcic melts.

Major Elements

The bulk compositions of model residual melts 3–4, formed after the crystallization of orthopyroxene and before the crystallization of plagioclase, are very similar to those of noncumulate eucrites (Table 4). These melts have Mg# (=100 Mg/[Mg + Fe)], MgO/SiO_2, CaO/Al_2O_3, and FeO/MnO ratios that bracket those of noncumulate eucrites (Table 4). The chrome contents of the model melts are clearly low compared to eucrites (Table 4), but this can be explained if MAGFOX overestimates the amount of early-crystallizing chromite, as noted above. The abundances of Al_2O_3 and CaO are somewhat low, and that of SiO_2 somewhat high, in melts 3–4 compared to eu-

TABLE 4. Major-element composition of magma ocean liquids initially and after 69% (melt 3) and 77% (melt 4) fractional crystallization, compared to eucrites.*

	initial	melt 3	melt 4	eucrites†
wt%				
SiO_2	45.34	50.87	49.66	48.07–49.53
TiO_2	0.18	0.46	0.62	0.56–0.96
Al_2O_3	3.29	8.65	11.83	11.78–13
Cr_2O_3	0.85	0.13‡	0.11‡	0.28–0.38
FeO	14.34	20.48	21.39	16.07–20.1
MnO	0.40	0.57	0.59	0.47–0.59
MgO	32.67	11.04	5.50	5.46–7.28
CaO	2.78	7.38	9.71	10.24–10.99
Na_2O	0.12	0.34	0.47	0.21–0.60
K_2O	0.01	0.03	0.04	0.03–0.08
P_2O_5	0.02	0.06	0.08	0.08–0.13
at%				
Mg/(Mg + Fe)	80	49	31	33–42
wt/wt				
MgO/SiO_2	0.72	0.22	0.11	0.11–0.15
CaO/Al_2O_3	0.84	0.85	0.82	0.80–0.88
FeO/MnO	36	36	36	29–39

*Assumes HED-CI starting composition, with residual melt compositions based on the MAGFOX program, developed by J. Longhi.
†Noncumulate, unbrecciated and monomict eucrites including: Béréba, Cachari, Camel Donga, Haraiya, Ibitira, Juvinas, Nuevo Laredo, Pasamonte, Sioux County, Stannern (BVSP, 1981; Jarosewich, 1990).
‡Probable underestimates (see text).

crites, but otherwise the agreement between the model and eucrites is remarkably good (Table 4). This is especially true considering the large fractionations (involving up to 77% crystallization) that must have occurred from the assumed starting composition.

Figure 4 shows the major-element compositions of the fractionating residual melts compared to eucrites in terms of MgO/SiO_2, CaO/Al_2O_3, and Mg#. Jurewicz *et al.* (1993, 1995) noted that such diagrams succinctly summarize the most important major-element ratios in eucrites. The fractionating magmas produced for the different model melt compositions given in Table 2 follow very similar trends (Fig. 4), showing the relative insensitivity of the models to the particular chondrite precursor assumed. In all cases, melts between stages 3 and 4 either approach or pass through the bulk compositions shown by noncumulate eucrites.

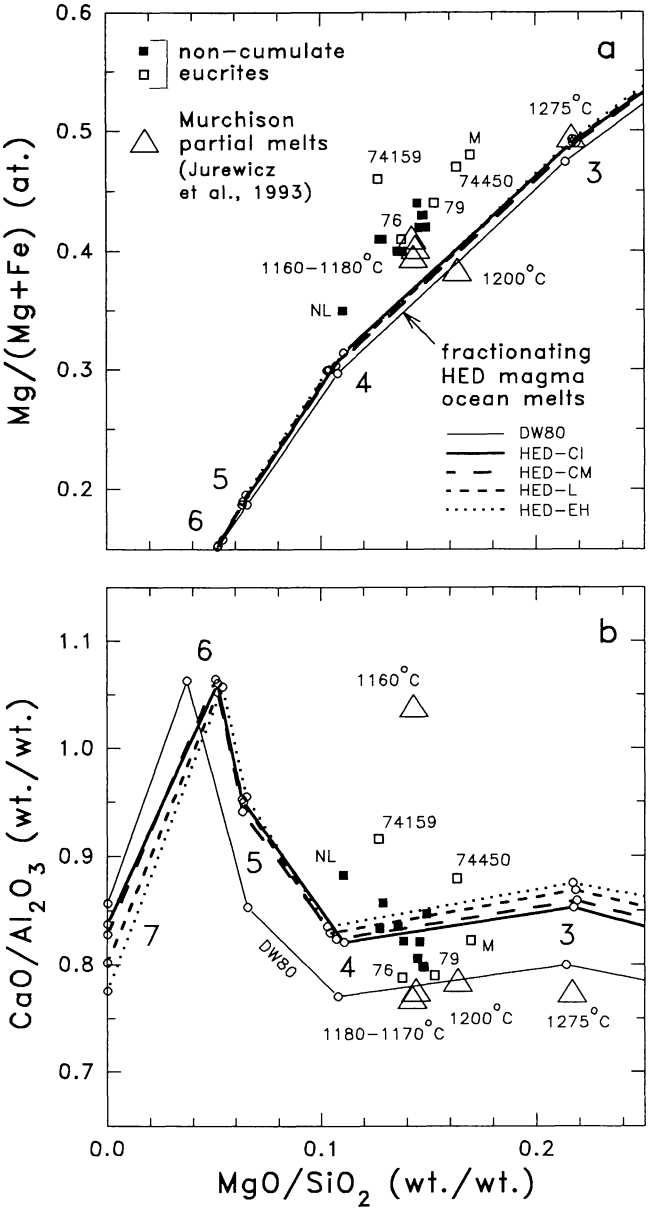

FIG. 4. Comparison of the major-element compositions for noncumulate eucrites with that of liquids in an HED magma ocean undergoing fractional crystallization. For the model trajectories, various initial compositions (given in Table 2) were assumed; inflections correspond to the appearance of new phases, as for the stages in Table 3. Triangles show the compositions of liquids at various temperatures produced by experimental melting of the Murchison CM chondrite (Jurewicz *et al.*, 1993). Eucrite data sources: unbrecciated and monomict eucrites (shaded squares), same as in Table 4; eucrites known or suspected to be polymict (unshaded squares), including ALHA76005 ("76"), Y-791195 ("79"), Y-74450, Y-74159, and Macibini ("M") (BVSP, 1981; Jarosewich, 1990).

For a given MgO/SiO_2 ratio, the models slightly underestimate Mg# compared to eucrites, and for the Dreibus and Wänke (1980) melt composition only, the CaO/Al_2O_3 ratio is slightly low compared to most eucrites (Fig. 4). The discrepancy in Mg# can be explained if the parent body has a higher Mg# than assumed. If the major-element compositions of diogenites were affected by late-stage reequilibration to produce somewhat more ferrous pyroxene, as seems likely (Mittlefehldt, 1994; Fowler *et al.*, 1994, 1995), the Mg# of the assumed starting compositions (Table 2) would be too low. Consequently, the small discrepancy in Mg# between the model melts and eucrites (Fig. 4) is readily understood.

Figure 4 also shows the melt compositions produced by experimentally melting the Murchison (CM) chondrite under reducing O fugacities at different temperatures (Jurewicz *et al.*, 1993). Jurewicz *et al.* (1993, 1995) suggested that experimental melts of Murchison provide a closer match to eucrites than experimental melts of other chondrite types, with the 1170 °C Murchison melt providing the best match of all. In Fig. 4, the experimental melt compositions appear to be very similar to that predicted by our models, especially for the Dreibus and Wänke (1980) starting composition, for experimental temperatures ≥1170 °C (Fig. 4). The 1160 °C melt has a CaO/Al_2O_3 ratio much *higher* than observed for eucrites and very different from our model melts; the 1170 °C melt has a CaO/Al_2O_3 ratio slightly lower than observed for most eucrites and lower than most of our model melts (Fig. 4). In contrast, the CaO/Al_2O_3 ratios of the HED-CI, HED-CM, HED-L, and HED-EH model melts all pass through the center of the eucrite field at the appropriate MgO/SiO_2 ratios, between stages 3 and 4 (Fig. 4). The 1170 °C Murchison melt does appear to provide a better match to eucrites in terms of Mg# (for a given MgO/SiO_2) than the model HED magma ocean melts, but this is probably because the initial Mg# values for the latter were slightly underestimated, as explained above.

Another noteworthy feature of Fig. 4 is the apparent tendency for unbrecciated and monomict noncumulate eucrites (filled squares) to form an apparent trend in the CaO/Al_2O_3 *vs.* MgO/SiO_2 plot roughly parallel to that expected for stage 4–6 melts (Fig. 4). Such "basaltic" eucrites provide a better estimate of liquid compositions than do polymict eucrites (unshaded squares in Fig. 4). The stage 4–6 model trend is produced by the cocrystallization of plagioclase and ferromagnesian minerals. Plagioclase crystallization is responsible for increasing the CaO/Al_2O_3 ratio of the residual melts, until augite joins the crystallization sequence at stage 6, at which point the trend is reversed (Fig. 4). Pigeonite crystallization between stages 4 and 6, olivine crystallization between stage 5 and 7, and augite crystallization between stages 6 and 7 are responsible for the steady decrease in the MgO/SiO_2 ratio as the melts crystallize (Fig. 4). The variation in the CaO/Al_2O_3 ratios of eucrites suggests that they experienced plagioclase fractionation, and the similarity of the eucrite data trend with that predicted for stage 4–5 or stage 4–6 melts suggests that the basaltic eucrites could have experienced partial equilibration with melts that evolved past stage 4. That plagioclase fractionation occurred in eucrites is also supported by rare-earth-element data, as discussed below, and by BVSP (1981).

To summarize, major-element data for eucrites are consistent with the hypothesis that eucrites formed as residual liquids in a magma

ocean setting. The magma ocean melts could have evolved by fractional crystallization roughly to the point at which plagioclase began to crystallize. Furthermore, it appears that the HED parent body could have roughly chondritic ratios of Al/Sc and Mg/Si, otherwise agreement between the model and observations would not be expected.

Rare Earth Elements

In this section, we combine estimates for mineral/melt partition coefficients (D-values) for rare-earth-elements (REE; Table 5) with the fractional crystallization model described above to model REE abundances in diogenites and eucrites (neglecting any effect of chromite, which is poorly handled in the model). We treat the initial REE abundance as a free parameter and discuss various initial concentrations in terms of the C_o parameter introduced earlier, where C_o = CI-chondrite normalized abundance of elements in the HED parent body. As previously discussed, values of $C_o > 1$ are likely for refractory trace elements such as the REE, based on the inferred depletion of volatile elements in the parent body (Dreibus *et al.*, 1977; Morgan *et al.*, 1978).

In the fractional crystallization model, orthopyroxene crystallizes between stages 1–3, and pigeonite alone crystallizes between stages 3–4. As shown above, the mineralogy and pyroxene composition of diogenites corresponds approximately to stage 3 pyroxene. Figure 5 shows that the REE abundances of diogenite orthopyroxene (Mittlefehldt, 1994; Fowler *et al.*, 1995) resemble stage 2–4 pyroxene, assuming $C_o \sim 3$. This agrees with the data presented in Fig. 3a. If the $D_{REE}^{opx/melt}$ values of Weill and McKay (1975) are used, the agreement between stage 2 and 3 pyroxene with diogenites is excellent for all REE; whereas, if the values of Schwandt and McKay (1996) are used, the agreement is less satisfactory for the light REE (LREE) but still excellent for the heavy REE (HREE) (Fig. 5). The overall similarity in the predicted and observed REE patterns and abundances supports the idea that diogenites formed as cumulates in a magma ocean. The agreement between the model and observations is generally satisfactory for values of C_o for the REE ranging between ~2.5–3.5.

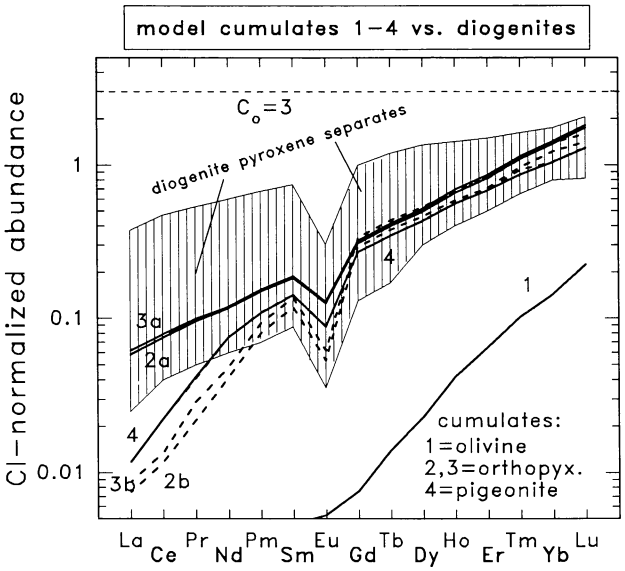

FIG. 5. Comparison of REE abundances in model cumulates 1–4 (heavy solid and dashed lines) with that of diogenite pyroxene separates (Mittlefehldt, 1994). Cumulates 1–4 correspond to the stages given in Table 3 and assume an initial REE abundance of 3 × CI chondrites (C_o = 3). Two different REE patterns are shown for stage 2 and 3 orthopyroxene depending on the value of $D^{opx/melt}$ used, with "2a" and "3a" based on the values of Weill and McKay (1975) and "2b" and "3b" based on the values of Schwandt and McKay (1996). The average CI chondrite abundances of Anders and Grevesse (1989) were used for normalization.

TABLE 5. Mineral/melt partition coefficients assumed in this work.

	Olivine	Orthopyroxene	Pigeonite	Plagioclase
Sc	0.13*, .24*	0.65#	1.50¥	0.0071¢
Cr	0.6†, 1.2‡	1.29, 1.83$	5.2¤	0.0332¢
La	0.0001§	0.007@, 0.0009&	0.0009£	0.0418¢
Ce	0.0001§	0.009@, 0.0014&	0.0017£	0.0302¢
Nd	0.0001§	0.014@, 0.0050&	0.0058£	0.0236¢
Sm	0.0006§	0.022@, 0.0142&	0.011£	0.0170¢
Eu	0.0007§	0.015@, 0.0064&	0.0068£	1.2¤
Gd	0.001§	0.037@, 0.0350&	0.021£	0.0105¢
Tb	0.002§	0.048@, 0.0454&	0.027£	0.0095¢
Dy	0.003§	0.060@, 0.0558&	0.034£	0.0089¢
Er	0.008§	0.10@, 0.0864&	0.055£	0.0077¢
Yb	0.019§	0.22@, 0.1512&	0.087£	0.0065¢
Lu	0.03§	0.22@, 0.1770&	0.11£	0.0068¢

*Colson *et al.* (1988). 1364 °C (for initial-stage 1) and 1202 °C (for stage 5–7), respectively.
†Weill and McKay (1975). Temperature 1380 °C, "FMG" composition (for initial-stage 1).
‡McKay and Weill (1976). 1200 °C (for stage 5–7).
§McKay (1986). Lanthanum and Ce assumed to be the same as for Nd; Eu, Tb, Dy, Er values interpolated.
#Colson *et al.* (1988), 1281 °C.
$Barnes (1986) 1305 °C (for stage 1–2) and 1255 °C (for stage 2–3), respectively, with fO_2 = IW.
@Weill and McKay (1975), 1200 °C run and as estimated from their Fig. 6. Europium anomaly assumed to be similar to that of pigeonite.
&Schwandt and McKay (1996). "High D." Gadolinium and Tb values interpolated.
¥Colson *et al.* (1988), 1202 °C run.
¤Weill and McKay (1975).
£McKay *et al.* (1991), Wo_5, fO_2 = IW. Lanthanum, Tb, Dy, Er, Lu values interpolated.
¢Phinney and Morrison (1990). Neodymium, Gd, Dy, Er values interpolated.

The agreement between model orthopyroxene and diogenites for the LREE using the Weill and McKay (1975) D-values may be fortuitous. The higher $D_{LREE}^{opx/melt}$ values of Weill and McKay (1975) compared to Schwandt and McKay (1996) and to the $D_{LREE}^{pig/melt}$ values of McKay *et al.* (1991) (Table 5) are suspect, because they were obtained before the effects of secondary fluorescence from an REE-enriched groundmass on REE-depleted minerals were fully recognized (McKay, 1986; McKay *et al.*, 1990, 1991). If the $D_{REE}^{opx/melt}$ values of Schwandt and McKay (1996) are adopted, it would appear that diogenite pyroxene has an excess of LREE over that predicted by the model. Both bulk analyses of pyroxene separates (Mittlefehldt, 1994) and SIMS analyses of individual pyroxene grains (Fowler *et al.*, 1995) show the apparent LREE excess.

Another puzzling aspect of the data is the large range in REE abundances shown by diogenites compared to the model predictions (Fig. 5). In part, this is almost certainly caused by the unrealistic assumption, made in the model, that partition coefficients are constant and do not vary with changing temperature or melt composition. However, even for models in which $D_{REE}^{px/melt}$ values vary modestly (factor of ~3) during orthopyroxene crystallization, the range in REE abundances within diogenite pyroxene is difficult to explain unless extensive amounts of pyroxene crystallization (~90%) are invoked (Fowler *et al.*, 1995). Such large amounts of crystallization are higher than what would be predicted by the model discussed here

(~21% from stage 1 to 3; ~41% from stage 1 to 4). Clearly, the issues of elevated LREE abundances and the large range in REE abundances in diogenites warrant further study.

Although the exact choice for $D_{REE}^{px/melt}$ values is critical for modelling REE abundances in pyroxene cumulates, it does not significantly affect the composition of the model residual liquids, as the values for these coefficients are so low (Table 5). Figure 6 compares the REE abundances of model liquids produced assuming $C_o = 3$ (the same as in Fig. 5) with that of a representative sampling of noncumulate eucrites. On the scale of the figure, there is no difference in melt compositions produced by assuming the different $D_{REE}^{opx/melt}$ values of Weill and McKay (1975) and Schwandt and McKay (1996).

Assuming $C_o \sim 2.5$–3.5, the REE data for noncumulate eucrites are consistent with stage 3–4 and post-stage–4 melts (Fig. 6). Eucrites with the lowest REE abundances (~9–13 × CI chondrites), such as Y-82066, Sioux County, Juvinas, and ALH-765, have relatively flat REE patterns with no negative Eu anomalies and appear to correspond to model residual melts 3–4. Eucrites with intermediate REE abundances (~13–16 × CI chondrites), such as Pasamonte, Chervony Kut, Lakangoan, and Nuevo Laredo, appear to have small negative Eu anomalies, as expected for melts that experienced plagioclase fractionation, soon after stage 4 (Fig. 6). Bouvante and Stannern have the highest REE abundances (~20–30 × CI chondrites), show prominent negative Eu anomalies, and appear to have HREE-depleted patterns (Fig. 6). Their REE abundances are very similar to that expected for stage 5–6 residual melts. While Bouvante and Stannern could correspond to stage 5–6 residual melts, other evidence described in the next section suggests that their origin was different than that of other noncumulate eucrites.

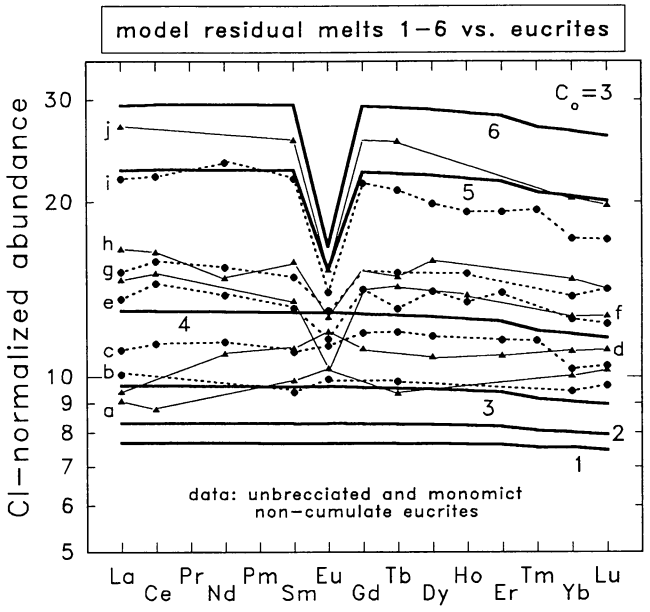

FIG. 6. Comparison of REE abundances in model residual liquids 1–6 (heavy lines) with that of selected eucrites. Liquids 1–6 correspond to the stages given in Table 3 and assume an initial REE abundance of 3 × CI chondrites ($C_o = 3$). Noncumulate eucrite data represent average concentrations for individual meteorites and include: (a) Y-82066 (Mittlefehldt and Lindstrom, 1993); (b) Sioux County (Palme and Rammensee, 1981; Palme *et al.*, 1978; Mittlefehldt, 1979), Ce data omitted; (c) Juvinas (Schmitt *et al.*, 1964; Wänke *et al.*, 1972; Palme and Rammensee, 1981; Shimuzu and Masuda, 1986; Nakamura and Masuda, 1980; Schnetzler and Philpotts, 1969); (d) ALH-765 (Nakamura and Masuda, 1980), Ce data omitted; (e) Pasamonte (Wänke *et al.*, 1977; Gast *et al.*, 1970; Mittlefehldt, 1979); (f) Chervony Kut (Palme *et al.*, 1978), Dy data omitted; (g) Lakangoan (Warren and Jerde, 1987); (h) Nuevo Laredo (Warren and Jerde, 1987), Dy data omitted; (i) Stannern (Schmitt *et al.*, 1964; Palme and Rammensee, 1981; Gast *et al.*, 1970; Mittlefehldt, 1979; Schnetzler and Philpotts, 1969); (j) Bouvante (Palme and Rammensee, 1981). The average CI chondrite abundances of Anders and Grevesse (1989) were used for normalization.

In general, the REE data for noncumulate eucrites are consistent with these meteorites having formed as residual liquids in a magma ocean. As the same values of C_o (~2.5–3.5) are consistent with the data for both diogenites (Fig. 5) and noncumulate eucrites (Fig. 6), this supports the idea that both types of meteorites originated in melts of the same or similar starting compositions. Moreover, the REE data for eucrites support the conclusion that some eucritic melts evolved approximately to stage 3–4 and that other eucritic melts evolved past the plagioclase crystallization step at stage 4.

Mg# Versus Samarium

Not *all* eucrites formed in the same way. Cumulate eucrites clearly formed as cumulates and do not represent liquid compositions, and not all noncumulate eucrites appear to have formed as residual liquids in a magma ocean. That this is the case is perhaps best seen in variation diagrams such as Fig. 7, in which a compatible element or parameter (*e.g.*, Mg#) is plotted against an incompatible element (*e.g.*, Sm). Similar diagrams were used by Warren and Jerde (1987) to argue that *most* noncumulate eucrites originated predominantly as residual liquids. In Fig. 7, the compositional trends of fractionating HED magma ocean liquids with C_o values of 2.5, 3.0, and 3.5 are shown, with Mg# based on Longhi's MAGFOX program and Sm based on the modelling discussed in the last section. Of the 20 noncumulate eucrites shown in Fig. 7, 16 have compositions that lie close to the trends expected for an origin as residual melts, which is consistent with the conclusions of Warren and Jerde (1987). This suggests that most, but not all, of the noncumulate eucrites in our collections could have formed as residual liquids in a magma ocean.

In Fig. 7, only the cumulate eucrites, and only the noncumulate eucrites Bouvante (Bo), Stannern (St), ALHA81001 (81), and Pomoz-

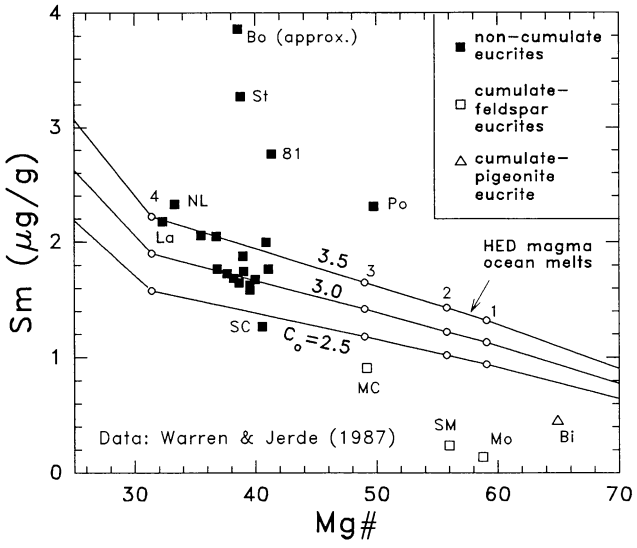

FIG. 7. Comparison of the Sm concentrations and Mg# (= 100 Mg/(Mg + Fe) atomic) values for eucrites with that of residual melts in an HED magma ocean undergoing fractional crystallization (HED-CI model). For the melt-composition trajectories, various initial Sm abundances were assumed, corresponding to initial CI-normalized abundances (C_o values) of 2.5, 3.0 and 3.5. Numbers along the composition trajectories correspond to the stages in Table 3. Eucrite data source: Warren and Jerde (1987).

dino (Po), lie off the expected trends for magma ocean melts. The latter noncumulate meteorites are members of the so-called "Stannern Trend," whereas, the other noncumulate eucrites in Fig. 7 belong either to the "Main Group" or the "Nuevo Laredo Trend" (Warren and Jerde, 1987). Candidates for magma ocean products, thus, include the Main Group and Nuevo Laredo Trend eucrites. The Stannern Trend eucrites formed differently, perhaps as partial melts (Warren and Jerde, 1987).

In detail, Fig. 7 provides additional evidence that noncumulate eucrites were generally affected by variable degrees of plagioclase fractionation. The compositions of the Main Group and Nuevo Laredo Trend eucrites generally scatter between the $C_o = 2.5$ and $C_o = 3.5$ trajectories (Fig. 7). Nuevo Laredo (NL) and Lakangoan (La) have compositions that correspond to model liquids close to stage 4 with $C_o \sim 3.5$; whereas, Sioux County (SC) has a composition corresponding to a model liquid between stages 3 and 4 with $C_o \sim 2.5$. That these eucrites do not plot along exactly the same C_o trend is probably indicative of a breakdown in the model, with some plagioclase fractionation occurring *before* the residual melt reached the low Mg/Si ratio and Mg# values appropriate for the onset of plagioclase crystallization at stage 4. This conclusion is consistent with the discussion regarding Ca/Al ratios and pyroxene compositions given above. Plagioclase fractionation will cause the Sm content of the liquid to change more rapidly for a given change in Mg# than expected for pigeonite fractionation alone, similar to the trend shown after stage 4 (left side of Fig. 7). If plagioclase fractionation is taken into account, most or all of the Main Group and Nuevo Laredo-Trend eucrites could have formed from a liquid with the *same* initial composition.

Owing to the apparent "model breakdown" close to stage 4, and the possibility that the initial Mg# of the melt may have been slightly underestimated (see above), it is difficult to estimate with precision which C_o value for the REE is most appropriate. However, the data bracket the melt trajectories for $C_o \sim 2.5$–3.5 (Fig. 7), which suggests that the value for C_o lies in this range. This value for C_o is consistent with the REE data for diogenites and eucrites (see above).

Chromium Versus Scandium

Jones and coworkers (Jones *et al.*, 1996; Jurewicz *et al.*, 1993, 1995) suggested that the moderately incompatible-compatible elements Cr, Sc, and V may be key to understanding the petrogenesis of eucrites. According to these authors, the Cr abundances of eucrites especially favor a partial melt origin, rather than a residual melt origin, for noncumulate eucrites (Jurewicz *et al.*, 1993; Jones *et al.*, 1996).

To see whether the data for moderately compatible-incompatible elements are consistent with a magma ocean hypothesis, we have used the same approach as for the REE to model the abundances of Cr and Sc in eucrites. We focused on Cr and Sc, as D_{Cr} and D_{Sc} for the relevant phases and temperatures encountered in a magma ocean appear to be reasonably well known. For olivine and pyroxene, D_{Cr} and D_{Sc} increase as temperature decreases (Table 5), with the result that these elements change from somewhat incompatible to somewhat compatible, as olivine and pyroxene crystallize in a magma ocean. For the fractional crystallization model discussed in this paper, the amount of chromite that crystallizes early is uncertain (as noted above). Thus, modelling results involving Cr and Sc, which are highly compatible or moderately incompatible in chromite, respectively, are subject to ambiguity. In the models, the presence of early crystallizing chromite is neglected, and only orthopyroxene is assumed to crystallize between stages 1 and 3. Therefore, the Cr and Sc abundances in early formed (chromite-bearing) cumulates may be underestimated, while the Cr and Sc abundances in residual melts may be overestimated.

Figure 8 shows the abundances of Cr and Sc in model residual melts 1–6 for three different values of initial concentrations (2.0, 2.5 and 3.0 × CI chondrites for both elements). For these initial concentrations, the model liquid composition trajectories intersect the field of noncumulate eucrite compositions near stage 4 (Fig. 8). Therefore, Cr and Sc data for eucrites are consistent with the residual-liquid hypothesis. Moreover, that the eucrite data for Cr and Sc correspond to stage 4 liquids is consistent with all of the evidence discussed above. If the presence of some early crystallizing chromite is taken into account, the model residual melt compositions will shift to lower Sc and Cr abundances, and this will shift the value of the apparent C_o that matches the eucrite data ($C_o \sim 2$–3 assuming no chromite fractionation; Fig. 8) to higher values ($C_o \geq 2$–3). Such a shift will not appreciably change the conclusion that eucrites correspond roughly to stage 4 model liquids (Fig. 8). Initial Sc and Cr abundances of ≥2–3 × CI chondrites (assuming some chromite fractionation) in the HED parent body are implied.

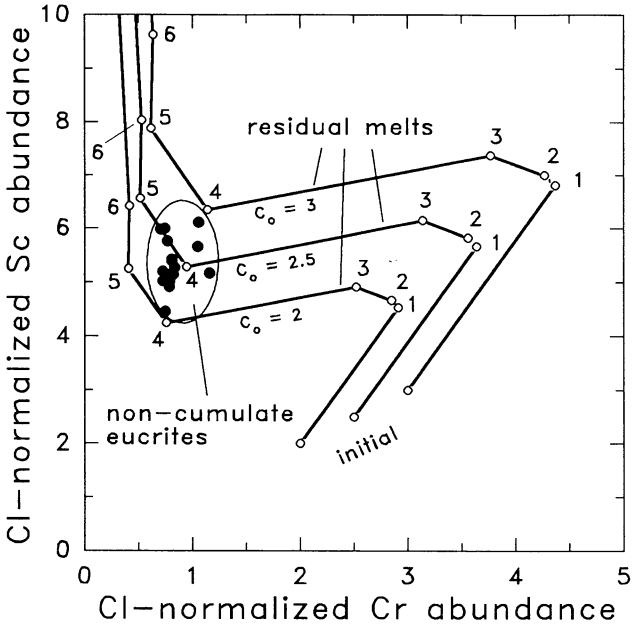

FIG. 8. Comparison of the CI-normalized abundances of Cr and Sc in diogenites and in unbrecciated and monomict noncumulate eucrites with model residual melts 1–7 produced by fractional crystallization. Numbers along the composition trajectories correspond to the stages in Table 3. Eucrite data points represent average concentrations for individual meteorites. The average CI chondrite abundances of Anders and Grevesse (1989) were used for normalization. Eucrite data: Bérèba (Palme *et al.*, 1978; Mittlefehldt, 1979; Schmitt *et al.*, 1972); Bouvante (Palme and Rammensee, 1981); Cachari (Palme *et al.*, 1978; Schmitt *et al.*, 1972); Chervony Kut (Palme *et al.*, 1978; Schmitt *et al.*, 1972); Ibitira (Morgan *et al.*, 1978; Wänke *et al.*, 1972, 1974; Palme and Rammensee, 1981; Jarosewich, 1990); Juvinas (Wänke *et al.*, 1972; Palme and Rammensee, 1981; Schmitt *et al.*, 1964, 1972); Haraiya (Mason *et al.*, 1979; Schmitt *et al.*, 1972); Lakangaon (Warren and Jerde, 1987; Schmitt *et al.*, 1972); Nuevo Laredo (Warren and Jerde, 1987; Schmitt *et al.*, 1972); Pardvarninkai (Mason *et al.*, 1979; Schmitt *et al.*, 1972); Pasamonte (Wänke *et al.*, 1972; Palme and Rammensee, 1981; Mittlefehldt, 1979; Schmitt *et al.*, 1972); Perimiho (Schmitt *et al.*, 1972); Sioux County (Palme *et al.*, 1978; Palme and Rammensee, 1981; Mittlefehldt, 1979; Schmitt *et al.*, 1972); Stannern (Palme and Rammensee, 1981; Mittlefehldt, 1979; Schmitt *et al.*, 1972); ALHA81001 (Warren and Jerde, 1987); Y-82066 (Mittlefehldt and Lindstrom, 1993); Y-793164 (Mittlefehldt and Lindstrom, 1993).

We also modelled the abundances of Cr and Sc in the cumulates produced by fractional crystallization to see if the predicted orthopyroxenitic cumulates correspond to diogenites. In contrast to the eucrites, bulk analyses of diogenites show highly variable Cr abundances, which range over an order of magnitude (from ~1.5 to ~19 × CI chondrites, although mainly <3.5 × CI). This may indicate that various amounts of chromite were analyzed in sample sizes too small to be representative for these (rather coarse-grained) rocks. The Sc content of diogenites is less variable, ranging from ~2 to ~3.5 × CI chondrites. Unfortunately, the large variation in Cr content makes it difficult to assess how closely the model pyroxene cumulates correspond to diogenites. Nonetheless, the observed compositions seem to substantially overlap model stage 1–2 orthopyroxene cumulates assuming $C_0 \sim 2$–3. If $C_0 \sim 2$, a stage 3 orthopyroxene cumulate is also possibly consistent with the data. The presence of any early crystallizing chromite would appear to shift the model cumulate compositions to higher values of Sc and Cr, improving the agreement between diogenites and stage 1 cumulates, and worsening the agreement between diogenites and stage 2 and 3 cumulates.

The data for Sc and Cr, which represent moderately incompatible-compatible elements, are consistent with the data for compatible elements (including major-elements) and with the data for incompatible elements (including the REE). The mineral/melt partition coefficients for these different elements in the relevant phases vary over a few orders of magnitude. Yet the conclusion is the same regardless of which element one models. Namely, it appears that diogenites and eucrites could have formed in the same, chemically evolving magmatic system, such as a magma ocean.

Pseudoternary Diagram

The partial melt hypothesis of eucrite formation gained support after it was realized that the compositions of noncumulate eucrites cluster around a pseudoperitectic for olivine, pigeonite, and plagioclase (Stolper, 1977). At low (*e.g.*, 1 bar) pressures, this pseudoperitectic composition will not be attained by liquids undergoing fractional crystallization that are also capable of producing diogenites. (However, see Warren, 1985 and Hewins and Newsom, 1988.) In contrast, the pseudoperitectic composition can be attained by low-pressure partial melting of a source containing olivine, low-Ca pyroxene, and plagioclase.

The relevant phase equilibria were reinvestigated by Longhi and Pan (1987), Bartels and Grove (1991), and Grove and Bartels (1992), all of whom concluded that noncumulate eucrites could have formed as residual liquids during fractional crystallization at elevated pressure. This elevated pressure was variously estimated as 2 ± 1 kb (Longhi and Pan, 1988), ~1 kb (Bartels and Grove, 1991), and ~0.5 kb (Grove and Bartels, 1992). If pressures much greater than 1 kb are required for fractional crystallization, then either Vesta (with a maximum interior pressure of ~1 kb; Table 1) cannot be the eucrite parent body or eucrites cannot have formed as residual liquids in a magma ocean that also crystallized diogenites (or both).

We argue that the available data and phase equilibrium constraints are consistent with a fractional crystallization origin for eucrites at pressures sufficiently low for them to have originated in Vesta. Figure 9 shows the olivine-plagioclase-quartz pseudoternary diagram of Longhi and Pan (1988), together with the compositions of unbrecciated and monomict noncumulate eucrites. Longhi and Pan (1988) discussed melting and crystallization of a composition they termed "EPB3," derived by Dreibus *et al.* (1977). This composition represents an earlier iteration of the Dreibus and Wänke (1980) composition and is similar to the other compositions given in Table 2, especially the HED-CI composition.

For fractional crystallization of the HED-CI or EPB3 melts (heavy and thin solid lines in Fig. 9, respectively), the compositions of the residual liquids closely approach the compositions of eucrites at stage 4 (Fig. 9). This is especially true for fractional crystallization at 1 and 2 kb. As the errors associated with the 1 and 2 kb data are estimated to be ±1 kb by Longhi and Pan (1988), this would appear to allow fractional crystallization at pressures as low as 0–1 kb, which is within the pressure range of Vesta. For comparison, partial melting curves for the EPB3 composition (dotted lines in Fig. 9) imply a range of 0–5 kb to match eucrite compositions (Fig. 9). Pressures up to 5 kb are inconsistent with Vesta being the eucrite parent body.

Thus, for the pressures obtained within Vesta, it appears that the model parent body compositions given in Table 2 cannot easily produce noncumulate eucrite compositions through partial melting, but that they *can* produce noncumulate eucrite compositions by crystallization.

Stokes Settling Calculations and Equilibrium Crystallization

The apparent breakdown in the fractional crystallization model at large degrees of crystallization (corresponding roughly to the onset of plagioclase crystallization) suggests that crystals may not have been able to segregate from the melt, either because the magmas became choked with crystals (Tonks and Melosh, 1990; Taylor *et al.*,

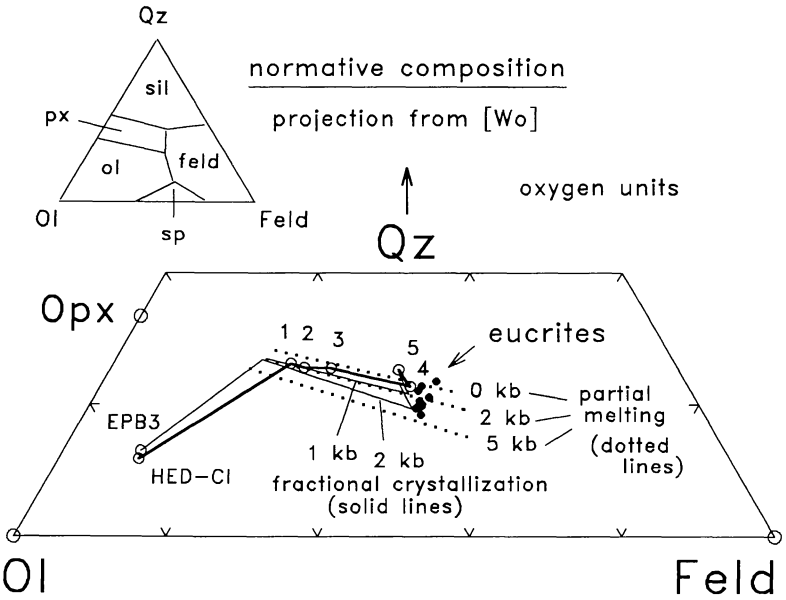

FIG. 9. Pseudoternary liquidus diagram olivine (Ol)-feldspar (Feld)-Quartz (Qz) comparing the compositions of noncumulate (unbrecciated and monomict) eucrites to hypothetical melt compositions produced by partial melting and fractional crystallization. The inset schematically illustrates the entire liquidus diagram. The heavy line shows the 1 bar, fractional crystallization trajectory of the HED-CI model melt of this work, with numbers corresponding to the stages given in Table 3. Thin lines show fractional crystallization trajectories at 1 kb and 2 kb for the similar "EPB3" composition (Dreibus *et al.*, 1977; Longhi and Pan, 1988). Dotted lines show the position of the cotectic/reaction boundary between olivine and low-Ca pyroxene appropriate to equilibrium partial melting of the EPB3 composition at 0, 2, and 5 kb. The projection scheme, EPB3 fractional crystallization trajectories, and EPB3 partial melting curves are after Longhi and Pan (1988). Eucrite data source: same as in Table 4.

1993) or because the viscosity of the melt became sufficiently large (or both). These possibilities can be evaluated by calculating Stokes flow settling velocities. For Stokes flow,

$$U_{\text{Stokes}} = \frac{2[\rho_f - \rho_s]ga^2}{9v} \quad \text{Eq. (4)}$$

where U = downward settling velocity of a spherical crystal, ρ_f = density of melt, ρ_s = density of crystal, g = gravitational acceleration, a = crystal radius, v = viscosity (Turcotte and Schubert, 1982, Eq. 6-229). Equation (4) shows that settling velocities depend on melt viscosity and density differences between the settling crystals and melt, and these parameters for the magma ocean fractionation model are plotted in Fig. 10. In Table 6, Stokes settling velocities calculated from Eq. (4) assuming a = 1 mm are given at various stages in the fractional crystallization of a magma ocean, neglecting the possibility of crystal-choking and the effects of turbulence. These calculations are oversimplified representations of the actual settling rates. However, they should give a reasonable indication of the *relative* settling rates of various phases at different stages of magma ocean solidification, for a given grain size.

Figure 10 and Table 6 show that melt viscosity increases dramatically between stages 3 and 4, just before plagioclase crystallizes. By the time that plagioclase crystallizes at stage 4, melt viscosities will have increased and the settling velocities will have decreased by an order of magnitude compared to stage 3 (Table 6). Table 6 suggests that early crystallizing phases such as Mg-olivine, Mg-orthopyroxene, and the most Mg-rich pigeonite will separate from melt relatively quickly compared to later crystallizing phases. Even late crystallizing Fe-olivine, although relatively dense (Fig. 10), would be expected to sink rather slowly because of high melt viscosities (Table 6). Plagioclase is less dense than melt and should float (Fig. 10), but it will move more slowly than other phases because of the small difference in density between it and melt and because of the high viscosity of coexisting melt (Table 6). This suggests that the formation of a plagioclase flotation crust on Vesta will be inhibited.

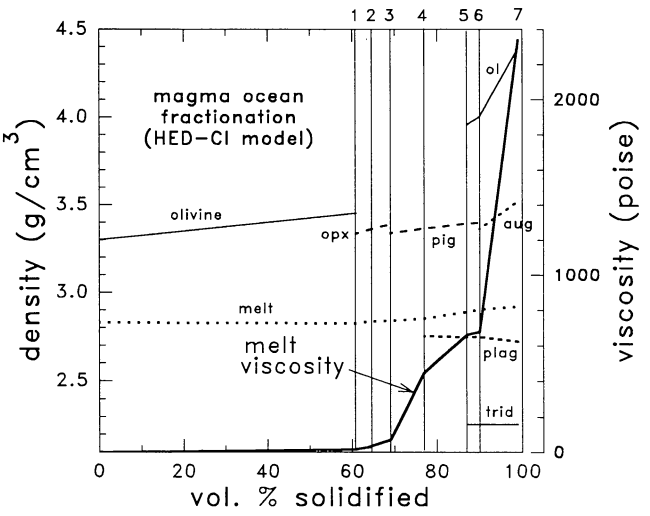

FIG. 10. Density of phases and melt viscosity as a function of percent magma crystallized during fractional crystallization of the HED-CI model magma. Numbers along the top of the plot correspond to the stages given in Table 3. Temperatures, phase compositions, and phase crystallization intervals were determined with the MAGFOX program, written by J. Longhi; densities for minerals were estimated by interpolating density data from Deer *et al.* (1966) for endmember compositions; and melt densities and viscosities were determined with the DENSITYBW and VISCOSTY programs, respectively, of P. Warren. The large increase in melt viscosity after ~70% solidification will limit the ability of late crystallizing phases to sink or float in the magma.

Marsh and Maxey (1985) suggested that although both crystal settling rate and convection rate decrease with increasing magma viscosity, the overall effect of increasing melt viscosity is to inhibit crystal-melt separation. Thus, the apparent breakdown in the fractional crystallization model slightly before the plagioclase crystallization step (stage 4) can be attributed, at least in part, to the incomplete separation of phases caused by high melt viscosities. Crystal-choking at high degrees of magma ocean solidification also may have inhibited fractional crystallization.

Owing to the likelihood of inefficient crystal-liquid separation at high degrees of crystallization, it is assumed that the last stages of magma ocean crystallization will be dominated by an *approach* to equilibrium crystallization conditions. As crystal settling velocities become especially low between stages 3 and 4, we consider equilibrium crystallization for melt compositions corresponding to those obtained at stages 3 and 4. Longhi's companion program to MAGFOX for equilibrium crystallization, MAGPOX, was used to determine the 1 bar equilibrium crystallization assemblages and residual melt compositions produced for stage 3 and 4 liquids.

The residual melt compositions produced by equilibrium crystallization are similar to those produced by fractional crystallization, except at the most evolved compositions. The equilibrium crystallization assemblages of melts 3 and 4 are dominated by plagioclase (39–55 vol%, An_{88}) and pigeonite (50–16%, $En_{50-43}Wo_6$), with smaller amounts of silica polymorph (3–5%), and appreciable amounts of ferrous olivine (9–23%, Fo_{26-20}). For comparison, noncumulate eucrites typically contain 41–42% plagioclase (An_{80-90}), 53–56% pigeonite (En_{35-48}), 1–4% silica polymorph, and 1% chromite (BVSP, 1981). Although the amount of olivine is clearly overestimated, the overall similarity between the model and noncumulate eucrites is generally consistent with the idea that eucrites could have crystallized under quasi-equilibrium-crystallization conditions in a magma ocean, following the formation of diogenites by fractional crystallization.

TABLE 6. Melt viscosities (v_{melt}) and Stokes settling velocities (U_{Stokes}) for minerals in a Vesta-wide magma ocean undergoing fractional crystallization (HED-CI model).

Mineral, melt stage*	$\Delta\rho$ (g/cm^3)†	v_{melt} (Poise)‡	U_{Stokes} (m/year)§
ol, initial	0.47	0.4	21500
ol, 1	0.63	19	603
opx, 1	0.51	19	492
opx, 3	0.55	73	137
pig, 3	0.50	73	125
pig, 4	0.51	449	21
plag, 4	–0.10	449	–4
pig, 5	0.50	662	14
plag, 5	–0.14	662	–4
trid, 5	–0.63	662	–17
ol, 5	1.05	662	29

*Mineral symbols and melt stages as in Table 3; silica polymorph assumed to be tridymite (trid).
†Difference in density between mineral and melt (= density mineral–density melt), with melt densities found by using the program DENSITYBW by P. Warren.
‡Melt viscosity found by using the program VISCOSTY by P. Warren.
§Based on Eq. (4) in text. Assumes a grain radius of 1 mm and the surface gravity of Vesta.

Model for the Interior of Vesta

The differentiation model discussed above, together with constraints on the size of a metal core in Vesta, can be used to model the interior of Vesta if spherical symmetry is assumed. In Table 7, different interior models are presented depending on the size of a metal core and the amount of olivine in the asteroid. Figure 11 shows two plausible models for the interior of Vesta corresponding to different chondritic protoliths and a 5 wt% metal core.

A metal content of 5 wt% is considered to be the best estimate for Vesta but can range anywhere between 0–25 wt% (see above). This results in a metal core of 0–128 km radius (Table 7, Fig. 11).

As discussed above, it appears possible to form many HED lithologies by the solidification of a magma ocean in Vesta, assuming that solidification proceeded first by fractional crystallization and then by equilibrium crystallization. In Vesta, fractional crystallization would have produced an olivine-rich mantle overlain by a lower crust containing pyroxenitic material, which is similar to diogenites. Equilibrium crystallization would have produced an upper crust of gabbroic or basaltic composition, which is similar to noncumulate eucrites. It is assumed that diogenites correspond to the orthopyroxene cumulates produced during stages 1–3 and to the pigeonite cumulates produced during the first half (50 vol%) of stage 3–4 crystallization. Eucrites are assumed to correspond to the remaining melt. The precise "cut-off point" between diogenites and eucrites, halfway through the stage 3–4 crystallization interval, is somewhat arbitrary, but it is generally consistent with the data for pyroxene mineral compositions (Fig. 3) and melt compositions (Fig. 4, Table 4).

The olivine content in Vesta will vary depending on what type of chondritic protolith is assumed. The olivine content is maximized with a carbonaceous chondrite protolith and minimized with an enstatite chondrite protolith. The HED-CI and HED-EH model compositions (Table 2) are representative of plausible olivine-rich and olivine-poor compositions, respectively, for Vesta. These two compositions are assumed for the silicate portion of Vesta in Table 7 and Fig. 11.

TABLE 7. Model of a fully differentiated Vesta for three core sizes and two plausible endmember olivine contents.*

Unit	Olivine-rich (HED-CI)		Olivine-poor (HED-EH)	
	Depth to unit (km)	Thickness of unit (km)	Depth to unit (km)	Thickness of unit (km)
core = 0 mass%				
eucritic crust	0	26	0	42
diogenitic crust	26	14	42	43
olivine mantle	40	224	86	179
Fe-metal core	–	0	–	–
core = 5 mass%				
eucritic crust	0	26	0	41
diogenitic crust	26	13	41	42
olivine mantle	39	151	83	107
Fe-metal core	190	75	190	75
core = 25 mass%				
eucritic crust	0	23	0	37
diogenitic crust	23	12	37	35
olivine mantle	35	102	72	65
Fe-metal core	137	128	137	128

*Assumes 73 vol% (HED-CI) or 60 vol% (HED-EH) fractional crystallization of the silicate portion of the HED parent body to produce olivine and diogenitic cumulates, and solidification of the remaining liquid to produce eucritic materials. Vesta is assumed to be spherical with a 265 km radius.

For the olivine-rich case, the olivine mantle is ~100–225 km thick, the pyroxenitic lower crustal unit is ~12–14 km thick, and the gabbroic upper crustal unit is ~23–26 km thick (Table 7, Fig. 11). For the olivine-poor case, the olivine mantle is ~65–180 km thick, the pyroxenitic lower crust is ~35–43 km thick, and the gabbroic upper crust is ~37–42 km thick (Table 7, Fig. 11). The total thickness of "crust," including both the pyroxenitic and gabbroic lithologies, is between ~35–40 km for an olivine-rich Vesta and between ~72–85 km for an olivine-poor Vesta.

Vesta has the shape of an oblate spheroid with a large difference (~60 km) between its maximum and minimum radii (Table 1; Thomas *et al.*, 1996). If Vesta was originally spherical or near-spherical and attained its present shape by impact cratering, a large cross-section of the interior of Vesta could have been exposed. Significantly, the total thickness of the model crust (~35–85 km) is comparable to the difference between the maximum and minimum radii of Vesta (~60 km). This suggests that all of the pyroxenitic and gabbroic lithologies in a layered crust on Vesta could have been excavated or exposed by impacts, regardless of the exact size of a metal core or

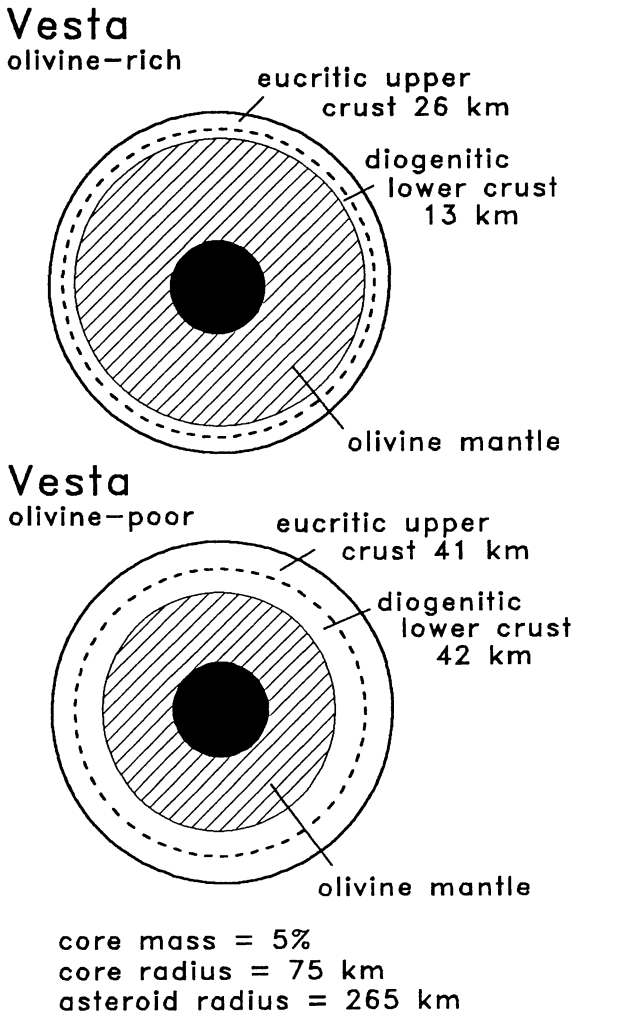

FIG. 11. Vesta interior models, drawn to scale, for two plausible endmember olivine contents and a fixed metal content of 5 wt%. Core dimensions and layer thicknesses for eucritic crust, diogenitic crust, and the olivine mantle are as in Table 7. Vesta is assumed to be spherical with a radius of 265 km.

the assumed type of chondritic protolith. If Vesta is olivine-rich, some mantle olivine also could have been exposed at the surface. Impact-excavation of mantle olivine would have been increasingly difficult if Vesta contained a lower proportion of olivine.

The Vesta interior models are generally consistent with (1) remote spectroscopic data for Vesta, which suggest that only small amounts of olivine are present on the surface (Gaffey, 1996); and (2) the assumption that little or none of the olivine in the HED parent body was sampled by HED meteorites (Dreibus *et al.*, 1977; Dreibus and Wänke, 1980). If the olivine detected spectroscopically on Vesta (Gaffey, 1996) corresponds to olivine derived from the mantle, this would imply that Vesta accreted from olivine-rich materials, which is perhaps similar to a volatile-depleted carbonaceous chondrite protolith.

DISCUSSION

Other Interior Models for Vesta and the Howardite, Eucrite and Diogenite Parent Body

Our models for a layered crust and mantle in the HED parent body and Vesta are similar to that advocated by Mason (1967), Takeda and coworkers (Takeda *et al.*, 1976, 1979; Takeda, 1979; Miyamoto and Takeda, 1977, 1994), and Delaney (1995), although they differ in detail.

Mason (1967) suggested that the eucrite parent body was differentiated into a eucritic crust (13 km thick), a diogenitic mantle (80 km thick), and a pallasitic olivine-metal core. The parent body was estimated to be 300 km in radius, so as to be consistent with inferred pallasite cooling rates. This overall structure (and diameter) is similar to what we infer for Vesta, except that Mason's diogenite mantle is much thicker, and his eucritic crust is much thinner. Furthermore, we do not propose that pallasites originated in the HED parent body. In our model, metal resides primarily in a core far from the surface of the asteroid and is unlikely to have been sampled, either in the form of pallasites or any other rock type.

Takeda and coworkers suggested that the gabbroic and pyroxenitic crust on the HED parent body is stratified into (from bottom to top) diogenites, cumulate-pigeonite eucrites, cumulate-feldspar eucrites, slowly cooled noncumulate eucrites, and rapidly cooled noncumulate eucrites. This would imply an inverted density sequence within the crust, as cumulate-feldspar eucrites are less dense (owing to their high feldspar content) than noncumulate eucrites. Cumulate-feldspar eucrites are inferred to have crystallized at ~8–12 km depth in the parent body (Miyamoto and Takeda, 1977, 1994), near the base of the eucritic crust. In our models, this depth is well within the eucritic crust, rather than at the base.

Delaney (1995) proposed that Vesta contains a 65-km-thick crust composed of an upper 25-km-thick eucrite layer and a lower 40-km-thick diogenite layer. This overall crustal thickness and stratigraphy is generally consistent with the models presented here, except that the proportion of diogenite to eucrite is larger in Delaney's model.

Grove and Bartels (1992) suggested that diogenites could have originated at great depth (~130 km) within Vesta, based on experiments suggesting that eucrites and diogenites could have been complementary differentiates from a melt at ≥0.5 kb pressure within the parent body. However, it is difficult to understand how diogenites could have been excavated from so deep within Vesta without also destroying much of the parent body and without delivering a large proportion of olivine to Earth in the form of meteorites.

Magma Oceans in Asteroids

Our results lend support to models that suggest that magma oceans may have been present within some asteroids (Taylor *et al.*, 1993). However, Taylor *et al.* (1993) concluded that magma oceans on asteroids would be turbulently convecting and that such turbulence would severely inhibit crystal settling, to the point that equilibrium crystallization would be expected to predominate over fractional crystallization. This is at odds with our conclusion that equilibrium crystallization was important only *after* fractional crystallization occurred to form diogenites and residual eucritic liquids.

Tonks and Melosh (1990) investigated magma ocean dynamics on the Earth and Moon. These researchers concluded that magma oceans on both the Earth and Moon would be turbulently convecting and that this would tend to favor equilibrium crystallization. However, they noted that crystal settling, and fractional crystallization, could still have occurred if the crystals grew to a large enough size. This would tend to promote fractional crystallization for early formed crystals, provided that such crystals could continue to grow as the magma ocean crystallized. Diogenites contain coarse orthopyroxene grains, up to 5 cm across in Johnstown (Mason, 1963), which suggests that the pyroxenes in diogenites grew to a large size before settling. Most important, Tonks and Melosh (1990) observed that crystal growth and fractional crystallization within a magma ocean would be promoted in *lower* gravity objects. This is because as gravity decreases, the rate-of-change in liquidus and solidus temperatures with depth becomes smaller and more similar to an adiabat, which potentially allows a crystal to continue to grow even while convection is occurring. For objects with high gravity, a crystal circulating to more shallow levels from deeper levels in a magma ocean would likely encounter the liquidus and would begin to melt, impeding its growth. As a result of this effect, Tonks and Melosh (1990) suggested that significant fractional crystallization could have occurred in a lunar magma ocean but that this was unlikely in a terrestrial magma ocean.

Based on the arguments of Tonks and Melosh (1990), it would seem that fractional crystallization in a magma ocean would be even more likely for Vesta than for the Moon, owing to the lower gravity of the former. Thus, despite the arguments of Taylor *et al.* (1993) to the contrary, significant fractional crystallization in a magma ocean on a Vesta-sized body appears to be possible.

SUMMARY

The HED achondrites provide valuable constraints on the HED parent body, assumed to be Vesta. Vesta may contain a metal core composing anywhere from ~0–25% of the mass of Vesta, with ~5 mass% representing the best estimate. An early magma ocean on Vesta is consistent with a large variety of data for eucrites and diogenites, including the mineralogy, pyroxene compositions, major-element compositions, REE abundances, and Cr and Sc abundances of these meteorites, as well as with phase equilibrium constraints and with Stokes settling calculations for the magma ocean. Modelling results suggest that the parent body is enriched in refractory elements such as the REE by ~2.5–3.5 × CI chondrites and that it has approximately chondritic Al/Sc and Mg/Si ratios. In a Vestan magma ocean, diogenites could have formed by fractional crystallization, and non-cumulate eucrites could have formed by quasi-equilibrium crystallization in the residual gabbroic liquid. A magma ocean would have resulted in an olivine mantle, a diogenitic lower crust, and an eucritic upper crust. Significant plagioclase flotation is not predicted and apparently did not occur in Vesta. In contrast, in the lunar magma ocean, equilibrium crystallization was followed by fractional crystallization involving significant plagioclase flotation (Snyder and Taylor, 1993). The reason for this difference is unclear,

but we speculate that differences in mass and size between the Moon and Vesta may have played a role.

Note added in proof: Based on recent imaging of Vesta with the Hubble Space Telescope, P. C. Thomas *et al.* (1997, *Science* **277,** 1492–1495) reported a refined size and shape model for Vesta and the discovery of a 460-km-diameter crater near the south pole of the asteroid. In the latest model, the uncertainty in the semi-major axes (radii) of Vesta (Table 1) is reduced to ±5 km from ±7 km. Systematic variations in spectral reflectance from floor-to-rim in the south pole crater suggest that Vesta is mineralogically stratified with depth, possibly consistent with the model reported here.

Acknowledgements–We thank John Jones, Horton Newsom, and Paul Warren for constructive reviews that greatly improved the quality of this manuscript, John Longhi for use of the MAGFOX and MAGPOX computer programs he developed, and Paul Warren for the use of his DENSITYBW and VISCOSTY computer programs. This paper was supported by NASA grant NAGW 3453.

Editorial handling: P. Warren

REFERENCES

ANDERS E. AND GREVESSE N. (1989) Abundances of the elements: Meteoritic and solar. *Geochim. Cosmochim. Acta* **53,** 197–214.

BARNES S. J. (1986) The distribution of chromium among orthopyroxene, spinel and silicate liquid at atmospheric pressure. *Geochim. Cosmochim. Acta* **50,** 1889–1909.

BARTELS K. S. AND GROVE T. L. (1991) High-pressure experiments on magnesian eucrite compositions: Constraints on magmatic processes in the eucrite parent body. *Proc. Lunar Planet. Sci. Conf.* **21st,** 351–365.

BASALTIC VOLCANISM STUDY PROJECT (BVSP) (1981) *Basaltic Volcanism on the Terrestrial Planets.* Pergamon Press, New York, New York. 1286 pp.

BINZEL R. P. (1996) Astronomical evidence linking Vesta to the HED meteorites: A review. In *Workshop on the Evolution of Igneous Asteroids: Focus on Vesta and the HED Meteorites* (eds. D. W. Mittlefehldt and J. J. Papike), p. 2. Lunar and Planetary Institute, Houston, Texas.

BINZEL R. P. AND XU S. (1993) Chips off of asteroid 4 Vesta: Evidence for the parent body of basaltic achondrite meteorites. *Science* **260,** 186–191.

BOWMAN L. E., PAPIKE J. J. AND SPILDE M. N. (1996) Modal abundances in diogenites: Insights into phase percentages using electron microprobe techniques (abstract). *Lunar Planet. Sci.* **27,** 147–148.

BRITT D. T. AND CONSOLMAGNO G. J. (1997) The porosity of meteorites and asteroids: Results from the Vatican collection of meteorites (abstract). *Lunar Planet. Sci.* **28,** 159–160.

BUNCH T. E. (1975) Petrography and petrology of basaltic achondrite polymict breccias (howardites). *Proc. Lunar Sci. Conf.* **6th,** 469–492.

CHOU C. L., BOYNTON W. V., BILD R. W., KIMBERLIN J. AND WASSON J. T. (1976) Trace element evidence regarding a chondritic component in howardite meteorites. *Proc. Lunar Planet. Sci. Conf.* **7th,** 3501–3518.

CLAYTON R. N. AND MAYEDA T. K. (1996) Oxygen isotope compositions of achondrites. *Geochim. Cosmochim. Acta* **60,** 1999–2017.

COLSON R. O., MCKAY G. A. AND TAYLOR L. A. (1988) Temperature and composition dependencies of trace element partitioning: Olivine/melt and low-Ca pyroxene/melt. *Geochim. Cosmochim. Acta* **52,** 539–553.

CONSOLMAGNO G. J. AND DRAKE M. J. (1977) Composition and evolution of the eucrite parent body: Evidence from rare earth elements. *Geochim. Cosmochim. Acta* **41,** 1271–1282.

DEER W. A., HOWIE R. A. AND ZUSSMAN J. (1966) *An Introduction to Rock-forming Minerals.* Longman Group Ltd., London, U.K. 528 pp.

DELANEY J. S. (1995) 4 Vesta: A thick-skinned parent for basaltic achondrites (abstract). *Lunar Planet. Sci.* **26,** 329–330.

DELANEY J. S., PRINZ M. AND TAKEDA H. (1984) The polymict eucrites. *Proc. Lunar Planet. Sci.* **15th,** C251–C288.

DREIBUS G. AND WÄNKE H. (1980) The bulk composition of the eucrite parent asteroid and its bearing on planetary evolution. *Z. Naturforsch.* **35a,** 204–216.

DREIBUS G., KRUSE H., SPETTEL B. AND WÄNKE H. (1977) The bulk composition of the moon and eucrite parent body. *Proc. Lunar Sci. Conf.* **8th,** 211–227.

DUKE M. B. AND SILVER L. T. (1967) Petrology of eucrites, howardites and mesosiderites. *Geochim. Cosmochim. Acta* **31,** 1637–1665.

FOWLER G. W., PAPIKE J. J., SPILDE M. N. AND SHEARER C. K. (1994) Diogenites as crystal cumulates: Insights from orthopyroxene major and minor element chemistry. *Geochim. Cosmochim. Acta* **58,** 3921–3929.

FOWLER G. W., SHEARER C. K., PAPIKE J. J. AND LAYNE G. D. (1995) Diogenites as asteroidal cumulates: Insights from orthopyroxene trace element chemistry. *Geochim. Cosmochim. Acta* **59,** 3071–3084.

FUKUOKA T., BOYNTON W. V. AND SCHMITT R. A. (1977) Genesis of howardites, diogenites, and eucrites. *Proc. Lunar Sci. Conf.* **8th,** 187–210.

GAFFEY M. J. (1996) Asteroid spectroscopy: Vesta, the basaltic achondrites, and other differentiated asteroids. In *Workshop on the Evolution of Igneous Asteroids: Focus on Vesta and the HED Meteorites* (eds. D.W. Mittlefehldt and J. J. Papike), pp. 8–9. Lunar and Planetary Institute, Houston, Texas.

GAFFEY M. J. BELL J. F. AND CRUIKSHANK D. P. (1989) Reflectance spectroscopy and asteroid surface mineralogy. In *Asteroids II* (eds. R. P. Binzel, T. Gehrels and M. S. Matthews), pp. 98–127. Univ. Arizona Press, Tucson, Arizona.

GAST P. W., HUBBARD N. J. AND WEISMANN H. (1970) Chemical composition and petrogenesis of basalts from Tranquillity Base. *Proc. Apollo 11 Lunar Sci. Conf.* **2nd,** 1143–1163.

GROVE T. L. AND BARTELS K. S. (1992) The relation between diogenite cumulates and eucrite magmas. *Proc. Lunar Planet. Sci. Conf.* **22nd,** 437–445.

HAMET J., NAKAMURA N., UNRUH D. M. AND TATSUMOTO M. (1978) Origin and history of the adcumulate eucrite, Moama as inferred from REE abundances, Sm-Nd and U-Pb systematics. *Proc. Lunar Planet. Sci. Conf.* **9th,** 1115–1136.

HEWINS R. H. AND NEWSOM H. E. (1988) Igneous activity in the early solar system. In *Meteorites and the Early Solar System* (eds. J. F. Kerridge and M. S. Matthews), pp. 73–101. Univ. Arizona Press, Tucson, Arizona.

IKEDA Y. AND TAKEDA H. (1985) A model for the origin of basaltic achondrites based on the Yamato 7308 howardite. *Proc. Lunar Planet. Sci. Conf.* **15th,** C649–C663.

JAROSEWICH E. (1990) Chemical analyses of meteorites: A compilation of stony and iron meteorite analyses. *Meteoritics* **25,** 323–337.

JONES J. H. (1984) The composition of the mantle of the eucrite parent body and the origin of eucrites. *Geochim. Cosmochim. Acta* **48,** 641–648.

JONES J. H., TREIMAN A. H., JANSSENS M-J., WOLF R. AND EBIHARA M. (1988) Core formation on the Eucrite Parent Body, the Moon and the AdoR Parent Body (abstract). *Meteoritics* **23,** 276–277.

JONES J. H., PASLICK C. R. AND MCKAY G. A. (1990) Experimental constraints on the composition of the eucrite parent body (abstract). *Lunar Planet. Sci.* **21,** 581–582.

JONES J. H., MITTLEFEHLDT D. W., JUREWICZ A. J. G., LAUER H. V., HANSON B. Z., PASLICK C. R. AND MCKAY G. (1996) The origin of eucrites: An experimental perspective. In *Workshop on Evolution Igneous Asteroids: Focus on Vesta and the HED Meteorites* (eds. D. W. Mittlefehldt and J. J. Papike), p. 15. Lunar and Planetary Institute, Houston, Texas.

JUREWICZ A. J. G., MITTLEFEHLDT D. W. AND JONES J. H. (1993) Experimental partial melting of the Allende (CV) and Murchison (CM) chondrites and the origin of asteroidal basalts. *Geochim. Cosmochim. Acta* **57,** 2123–2139.

JUREWICZ A. J. G., MITTLEFEHLDT D. W. AND JONES J. H. (1995) Experimental partial melting of the St. Severin (LL) and Lost City (H) chondrites. *Geochim. Cosmochim. Acta* **59,** 391–408.

LONGHI J. AND PAN V. (1988) Phase equilibrium constraints on the howardite-eucrite-diogenite association. *Proc. Lunar Planet. Sci. Conf.* **18th,** 459–470.

LUGMAIR G. W. AND SHUKOLYUKOV A. (1997) ^{53}Mn-^{53}Cr isotope systematics of the HED parent body (abstract). *Lunar Planet. Sci.* **28,** 851–852.

MASON B. (1963) The Hypersthene Achondrites. *Am. Mus. Novitates* **2155,** 13 pp.

MARSH B. D. AND MAXEY M. R. (1985) On the distribution and separation of crystals in convecting magma. *J. Volcan. Geothermal Res.* **24,** 95–150.

MASON B. (1967) Meteorites. *American Scientist* **51,** 429–455.

MASON B., JAROSEWICH E. AND NELEN J. A. (1979) The pyroxene-plagioclase achondrites. *Smithson. Contrib. Earth Sci.* **22,** 27–45.

MCKAY G. A. (1986) Crystal/liquid partitioning of REE in basaltic systems: Extreme fractionation of REE in olivine. *Geochim. Cosmochim. Acta* **50,** 69–79.

MCKAY G. A. AND WEILL D. F. (1976) Petrogenesis of KREEP. *Proc. Lunar Sci. Conf.* **7th,** 2427–2447.

MCKAY G., WAGSTAFF J. AND LE L. (1990) REE distribution coefficients for pigeonite: Constraints on the origin of the mare basalt Eu anomaly (abstract). *Lunar Planet. Sci.* **21,** 773–774.

MCKAY G., LE L. AND WAGSTAFF J. (1991) Constraints on the origin of the mare basalt europium anomaly: REE partition coefficients for pigeonite (abstract). *Lunar Planet. Sci.* **22,** 883–884.

McKay G., Le L. and Wagstaff J. (1991) Constraints on the origin of the mare basalt europium anomaly: REE partition coefficients for pigeonite (abstract). *Lunar Planet. Sci.* **22,** 883–884.

Mittlefehldt D. W. (1979) Petrographic and chemical characterization of igneous lithic clasts from mesosiderites and howardites and comparison with eucrites and diogenites. *Geochim. Cosmochim. Acta* **43,** 1917–1935.

Mittlefehldt D. W. (1994) The genesis of diogenites and HED parent body petrogenesis. *Geochim. Cosmochim. Acta* **58,** 1537–1552.

Mittlefehldt D. W. and Lindstrom M. (1993) Geochemistry and petrology of a suite of ten Yamato HED meteorites. *Proc. NIPR Symp. Antarct. Meteor.* **6,** 268–292.

Miyamoto M. and Takeda H. (1977) Evaluation of a crust model of eucrites from the width of exsolved pyroxene. *Geochem. J.* **11,** 161–169.

Miyamoto M. and Takeda H. (1994) Evidence for the excavation of deep crustal material of a Vesta-like body from Ca compositional gradients in pyroxene. *Earth Planet. Sci. Lett.* **122,** 343–349.

Miyamoto M., Duke M. B. and McKay D. S. (1985) Chemical zoning and homogenization of Pasamonte-type pyroxene and their bearing on thermal metamophism of a Howardite Parent Body. *Proc. Lunar Sci. Conf.* **15th,** C629–C635.

Morgan J. W., Higuchi H., Takahashi H. and Hertogen J. (1978) A "chondritic" eucrite parent body: Inference from trace elements. *Geochim. Cosmochim. Acta* **42,** 27–38.

Morrison D. (1977) Asteroid sizes and albedos. *Icarus* **31,** 185–220.

Nakamura N. and Masuda A. (1980) REE abundances in the whole rock and mineral separates of the Allan Hills-765 meteorite. *Mem. Natl. Inst. Polar Res., Spec. Issue* **17,** 159–167.

Newsom H. E. (1985) Molybdenum in eucrites: Evidence for a metal core in the eucrite parent body. *Proc. Lunar Planet. Sci. Conf.* **15th,** C613–C617.

Newsom H. and Drake M. J. (1982) The metal content of the eucrite parent body: Constraints from the partitioning behavior of tungsten. *Geochim. Cosmochim. Acta* **46,** 2483–2489.

Newsom H. and Drake M. J. (1983) Experimental investigation of the partitioning of phosphorus between metal and silicate phases: Implications for the Earth, Moon and Eucrite Parent Body. *Geochim. Cosmochim. Acta* **47,** 93–100.

Palme H. and Rammensee W. (1981) The significance of W in planetary differentiation processes: Evidence from new data on eucrites. *Proc. Lunar Planet. Sci. Conf.* **12th,** 949–964.

Palme H., Baddenhausen H., Blum K., Cendales M., Dreibus G., Hofmeister H., Kruse H., Palme C., Spettel B., Vilcsek E. and Wänke H. (1978) New data on lunar samples and achondrites and a comparison of the least fractionated samples from the earth, the moon and the eucrite parent body. *Proc. Lunar Planet. Sci. Conf.* **9th,** 25–27.

Phinney W. C. and Morrison D. A. (1990) Partition coefficients for calcic plagioclase: Implications for Archean anorthosites. *Geochim. Cosmochim. Acta* **54,** 1639–1654.

Pun A. and Papike J. J. (1996). Unequilibrated eucrites and the equilibrated Juvinas eucrite: Pyroxene REE systematics and major, minor, and trace element zoning. *Am. Mineral.* **81,** 1438–1451.

Righter K. and Drake M. J. (1997a) Formation of eucrites and diogenites on a Vesta-sized asteroid: I. Core formation (abstract). *Lunar Planet Sci.* **28,** 1177–1178.

Righter K. and Drake M. J. (1997b) Formation of eucrites and diogenites on a Vesta-sized asteroid: II. Equilibrium crystallization of a chondritic magma ocean (abstract). *Lunar Planet Sci.* **28,** 1179–1180.

Ruzicka A., Snyder G. A. and Taylor L. A. (1997a) Could eucrites have formed as residual liquids in a magma ocean? (abstract). *Lunar Planet Sci.* **28,** 1213–1214.

Ruzicka A., Snyder G. A. and Taylor L. A. (1997b) Formation of eucrites and diogenites in a magma ocean on the HED parent body (abstract). *Lunar Planet Sci.* **28,** 1215–1216.

Schmitt R. A., Smith R. H. and Olehy D. A. (1964) Rare-earth, yttrium and scandium abundances in meteoritic and terrestrial matter–II. *Geochim. Cosmochim. Acta* **28,** 67–86.

Schmitt R. A., Goles G. G., Smith R. H. and Osborn T. W. (1972) Elemental abundances in stone meteorites. *Meteoritics* **7,** 131–213.

Schnetzler C. C. and Philpotts J. A. (1969) Genesis of the calcium-rich achondrites in light or rare-earth and barium concentrations. In *Meteorite Research* (ed. P. H. Millman), pp. 206–215. D. Reidel Publishing Co., Dordrecht, Holland.

Schubart J. and Matson D. L. (1979) Masses and densities of asteroids. In *Asteroids* (eds. T. Gehrels and M. S. Matthews), pp. 84–97. Univ. Arizona Press, Tucson, Arizona.

Schwandt C. S. and McKay G. A. (1996) REE partition coefficients from synthetic diogenite-like enstatite and the implications of petrogenetic modeling. In *Workshop on the Evolution of Igneous Asteroids: Focus on Vesta and the HED Meteorites* (eds. D. W. Mittlefehldt and J. J. Papike), pp. 25–27. Lunar and Planetary Institute, Houston, Texas.

Shimuzu H. and Masuda A. (1986) REE patterns of eucrites and their genetic implications. *Geochim. Cosmochim. Acta* **50,** 2453–2460.

Snyder G. A. and Taylor L. A. (1993) Constraints on the genesis and evolution of the Moon's magma ocean and derivative cumulate sources as supported by lunar meteorites. *Proc. NIPR Symp. Antarct. Meteor.* **6,** 246–267.

Standish E. M., Jr. and Hellings R. W. (1989) A determination of the masses of Ceres, Pallas, and Vesta from their perturbations upon the orbit of Mars. *Icarus* **80,** 326–333.

Stolper E. (1977) Experimental petrology of eucritic meteorites. *Geochim. Cosmochim. Acta* **41,** 587–611.

Takeda H. (1979) A layered crust model of a howardite parent body. *Icarus* **40,** 455–470.

Takeda H. (1996) Mineralogical records of early planetary processes of the HED parent body. In *Workshop on the Evolution of Igneous Asteroids: Focus on Vesta and the HED Meteorites* (eds. D. W. Mittlefehldt and J. J. Papike), pp. 30–31. Lunar and Planetary Institute, Houston, Texas.

Takeda H. and Mori H. (1985) The diogenite-eucrite links and the crystallization history of a crust of their parent body. *Proc. Lunar Planet. Sci. Conf.* **15th,** C636–C648.

Takeda H., Miyamoto M., Ishii T. and Reid A. M. (1976) Characterization of crust formation on a parent body of achondrites and the moon by pyroxene crystallography and chemistry. *Proc. Lunar. Sci. Conf.* **7th,** 3535–3548.

Takeda H., Miyamoto M., Ishii T., Yanai K. and Matsumoto Y. (1979) Mineralogical examination of the Yamato-75 achondrites and their layered crust. *Mem. Natl. Inst. Polar Res., Spec. Issue* **12,** 82–108.

Taylor G. J., Keil K., McCoy T., Haack H. and Scott E. R. D. (1993) Asteroid differentiation: Pyroclastic volcanism to magma oceans. *Meteoritics* **28,** 34–52.

Thomas P. C., Binzel R. P., Gaffey M. J., Zellner B. H., Storrs A. D. and Wells E. (1996) Vesta: Spin Pole, Size, and Shape from HST images. In *Workshop on the Evolution of Igneous Asteroids: Focus on Vesta and the HED Meteorites* (eds. D. W. Mittlefehldt and J. J. Papike), pp. 32–33. Lunar and Planetary Institute, Houston, Texas.

Tonks W. B. and Melosh H. J. (1990) The physics of crystal settling and suspension in a turbulent magma ocean. In *Origin of the Earth* (eds. H. E. Newsom and J. H. Jones), pp. 151–174. Oxford Univ. Press, New York, New York.

Turcotte D. L. and Schubert G. (1982) *Geodynamics: Application of Continuum Physics to Geological Problems.* John Wiley & Sons, New York, New York. 450 pp.

Wänke H. (1981) Constitution of terrestrial planets. *Phil. Trans. Roy. Soc. Lond. A* **303,** 287–302.

Wänke H., Baddenhausen H., Balacescu A., Teschke F., Spettel B., Dreibus G., Palme H., Quijano-Rico M., Kruse H., Wlotzka F. and Begemann F. (1972) Multielement analyses of lunar samples and some implications of the results. *Proc. Lunar Sci. Conf.* **3rd,** 1251–1268.

Wänke H., Palme H., Baddenhausen H., Dreibus G., Palme H., Jagoutz E., Kruse H., Spettel B., Teschke F. and Thacker R. (1974) Chemistry of Apollo 16 and 17 samples: Bulk composition, late stage accumulation and early differentiation of the moon. *Proc. Lunar Sci. Conf.* **5th,** 1307–1335.

Wänke H., Baddenhausen H., Blum K., Cendales M., Dreibus G., Hofmeister H., Kruse H., Jagoutz E., Palme C., Spettel B., Thacker R. and Vilcsek E. (1977) On the chemistry of lunar samples and achondrites. Primary matter in the lunar highlands: A reevaluation. *Proc. Lunar Sci. Conf.* **8th,** 2191–2213.

Warren P. H. (1983) Al-Sm-Eu-Sr systematics of eucrites and Moon rocks: Implications for planetary bulk compositions. *Geochim. Cosmochim. Acta* **47,** 1559–1571.

Warren P. H. (1985) Origin of howardites, diogenites and eucrites: A mass balance constraint. *Geochim. Cosmochim. Acta* **49,** 577–586.

Warren P. H. and Jerde E. A. (1987). Composition an origin of Nuevo Laredo Trend eucrites. *Geochim. Cosmochim. Acta* **51,** 713–725.

Wasson J. T. and Kallemeyn G. W. (1988) Compositions of chondrites. *Phil. Trans. Roy. Soc. Lond. A* **325,** 535–544.

Weill D. F. and McKay G. A. (1975) The partitioning of Mg, Fe, Sr, Ce, Sm, Eu, and Yb in lunar igneous systems and a possible origin of KREEP by equilibrium partial melting. *Proc. Lunar Sci. Conf.* **6th,** 1143–1158